Mineralogical and fluid inclusion characteristics of epithermal-style gold mineralization at the Goldy and Irene showings, Dawson Range, Yukon Territory, Canada

By

Robin Mann

A Thesis Submitted to

Saint Mary's University, Halifax, Nova Scotia

in Partial Fulfillment of the Requirements for

the degree of Bachelor of Science in Geology

April 2019, Halifax, Nova Scotia

Approved: Dr. Jacob Hanley
                     Examining Committee
Approved: Dr. Jarda Dostal
                     Reader

April 26, 2019

Mineralogical and fluid inclusion characteristics of epithermal-style gold mineralization at the Goldy and Irene showings, Dawson Range, Yukon Territory, Canada

By Robin Mann

Abstract

Jurassic- to Cretaceous-age gold mineralization at the Goldy and Irene showings in the Dawson Range, Yukon Territory occurs in intrusive igneous bodies and metasedimentary rocks of the Yukon-Tanana terrane. Petrography, fluid inclusion microthermometry, electron microprobe analysis, and SEM-BSE techniques were used to study the characteristics of Au mineralization. At the Goldy showing mineralization consists of: pyrite, arsenopyrite, chalcopyrite, (suspected) dissolved gold in sulfides, sphalerite, galena, +/- tetrahedrite-tennantite, +/- rutile and boulangerite in multiple stages of hydrothermal quartz-carbonate veining. At the Irene showing mineralization consists of: pyrite, arsenopyrite, chalcopyrite, galena, stibnite, electrum, rutile, boulangerite, and a variety of Sb-sulfides and sulfosalts hosted in quartz-carbonate veining. Fluid inclusion microthermometry of secondary inclusions hosted in quartz showed salinity ranges of 0-6 wt% NaCl eq at Goldy, and homogenization temperatures ($T_h^{L+V \to L}$) of 200-250 °C. At Irene salinity ranges of 5-15 wt% NaCl eq. and $T_h^{L+V \to L}$ of 140-230 °C were determined. The results of mineralogical and fluid inclusion studies suggest that the showings can be classified as low- (to intermediate)-sulfidation epithermal style mineralization. The dissimilarity of salinities and $T_h^{L+V \to L}$ values, with Irene being a cooler (and possibly deeper) hydrothermal system with higher salinities than Goldy indicates differing distances from a common heat source and more pronounced involvement of meteoric water at Goldy. Two different mineralizing events are proposed: a high T event involving As-Au association, and a lower T event, more consistent with epithermal T conditions involving Sb-Au association that is more pronounced at the Irene showing.

April 26, 2019

1

Acknowledgements

I would like to acknowledge Triumph Gold Corp. for giving me the opportunity to be part of their crew for the 2017 and 2018 drilling seasons on the Freegold property, Yukon. Several members of the crew became good friends and mentors. I would like to extend my gratitude to the Geology Department at Saint Mary's University. Many members of faculty and my fellow students were integral in development my continued fascination in the extensive subject of the Earth Sciences. I would like to thank my friend and supervisor, Dr. Jacob Hanley (Saint Mary's University), for his tireless support and mentorship that made this endeavour possible.

Table of Contents

List of Figures

List of Tables

1.0 Introduction

The objective of this study was to characterize and compare epithermal quartz-carbonate-Au-sulfide vein mineralization occurring at the Goldy and Irene showings (Triumph Gold Corporation Ltd.) in the Dawson Range, Yukon Territory, Canada. Specific goals of the study were (i) to determine if the two showings constitute parts of a single hydrothermal system with sporadic mineralized centers along a common structure, or in relation to a common heat source; (ii) to determine the hydrothermal fluid characteristics and crustal depth of gold mineralizing process(es); and (iii) to characterize the mineralogy expressed at the showings leading to a classification of the P-T regime of the mineralization.

Both showings contain significantly elevated Au concentrations of quartz-carbonate-sulfide veins that are focused along fault-modified contacts between the metamorphic rocks of the Yukon Tanana terrane and intrusive bodies that are Jurassic to Cretaceous in age. The Goldy showing comprises a roughly 160 x 160 metre, elliptical area of dense quartz stockwork veining at the contact between biotite schist/gneiss and Jurassic syenite. The Irene showing, located 9.5 km NW of Goldy, comprises a greater than 3-metre-thick quartz-sulfide vein exposed over 150 metre strike-length at a contact between biotite schist/gneiss and biotite-hornblende granodiorite-granite of probable mid- to late-Cretaceous age. At both showings, roughly fault/contact-parallel quartz-feldspar-porphyry dykes are present and are interpreted to occur along segments or splays associated with the regionally important Big Creek Fault (Matas et al., 2014).

Using petrographic microscopy, a paragenetic investigation of the mineralization (ore and accessory minerals) and associated alteration assemblages were conducted to better characterize these two showings. This was complemented by fluid inclusion analyses (petrography and microthermometry) of the vein-hosted minerals aimed at constraining fluid composition and origin, as well as the crustal depth and temperature of the mineralizing event(s). The value of this study will be to ultimately establish robust geochemical criteria to aid in mineral exploration in this under-characterized region.

2.0 Geological Setting

Located in northwestern Canada, the Yukon Territory has been a backbone of the Canadian economy and a pillar of the mineral exploration industry for over a hundred years. During the Klondike gold rush at the turn of the 20th century, thousands of prospectors migrated to the Yukon in the search of gold. This resource came in the form of placer deposits in and around Dawson City's rivers, streams, and estuaries. As the area became populated with prospectors, many began to venture south into the Dawson Range, an approximately 60-kilometer-long NW gold-endowed trend which includes Mount Nansen and Freegold Mountain (Fig. 1). The miners quickly recognized the placer gold grains were angular, indicating limited transport suggesting that the source was not too far away (LeBarge, 1995). To exploit the subsurface resources, a more sophisticated approach to mineral exploration that involved drilling and blasting was required. This activity revealed a variety of mineral deposit styles within the Dawson Range including porphyry copper-gold deposits and epithermal Au-Ag vein deposits, in addition to placer Au deposits (Smuck, 1999).

2.1 Dawson Range

The Dawson Range is part of the Intermontagne Belt of the northern Canadian Cordillera (Fig. 1). This section of the Canadian Cordillera is comprised of five tectonic terranes which accreted between the early Proterozoic and Cretaceous (Price, 1986). The margins of the Dawson Range are traced by two NW-trending fault systems: the Denali Fault in the south, and the Tintina fault to the north which accommodated strike-slip movement of up to 400km during accretional transpression (Bineli et al., 2016). This range is underlain by the heavily deformed Yukon-Tanana terrane comprised of mylonitic, metasedimentary, and meta-igneous schistose and gneissic rocks which are likely Devonian to Mississippian. Older pericratonic Yukon-Tanana rocks represent a composite of terranes that were accreted to the North American continent during early Mesozoic time (Colpron et al., 2006). Regional metamorphic grade varies from greenschist to amphibolite facies (Payne et al., 1987) and impacted most of central Yukon to western Alaska (Mortensen, 1992). The Yukon-Tanana terrane was intruded by several plutonic bodies and dykes that vary from granitic to granodioritic in composition.

The Big Creek Fault (Fig.1) is a major structure in the area and is considered genetically related to the numerous mineral deposits in the area, of suspected epithermal or porphyry affinity. This structure is a normal fault with a southwest-side down-motion and expresses an aeromagnetic anomaly that extends across the Freegold Mountain region (Carlson, 1987).
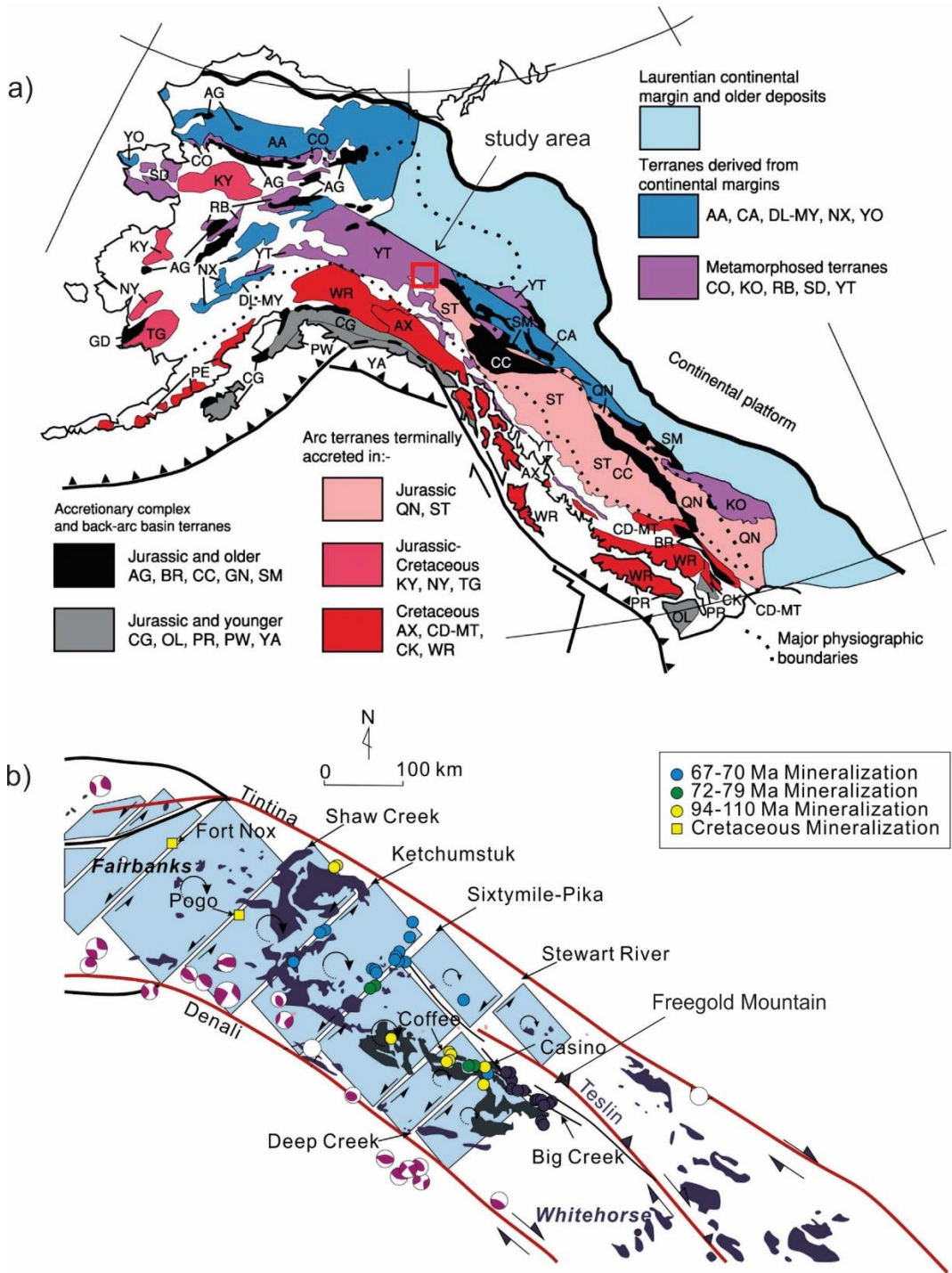
Figure 1. Terrane and structure maps. (a) Distribution, origins, and times of accretion of terranes. For the importance of this report YT = Yukon Tanana (purple) is the terrane of interest. (b) Map of the Denali-Tintina Fault Zone showing high-angle cross faults. Stereographic projections showing movement of structures and dots representing relative age of mineralization. Modified from Matas et al. (2014) showing spatially related mineral properties in relation to the Freegold Mountain property. Terrane names and descriptions

made by Monger et al (2004): Arctic Alaska (AA): former North American continental margin deposits, locally with Devonian plutons, possibly rifted away by counterclockwise rotation of ~70% from its former position near the Canadian Arctic Islands in Early Cretaceous time (~130Ma). Cassiar (CA): former North American continental margin deposits, sliced off and translated northwards by 425–2000km on right-lateral strike-slip faults. Coldfoot (CO), Kootenay (KO), Ruby (RB), Seward (SD), and Yukon Tanana (YT): derived mainly from Neoproterozoic and Early Palaeozoic rift and lower slope deposits, and Middle Devonian to Early Carboniferous continental margin arcs; metamorphosed and multiply deformed in Paleozoic, Mesozoic, and Paleogene times. Dillinger (DL), Mystic (MY), and Nixon Fork (NX): small terranes in Intermontane Alaska whose stratigraphy and Early and Middle Paleozoic faunas resemble those of the Siberian (or North Asian) craton margin.

Both mineral showings (Goldy and Irene) (Fig. 2) described in this study contain economically significant concentrations of gold in quartz-carbonate-sulfide veins that are located along fault-modified contacts between the metamorphic rocks of the Yukon-Tanana terrane and intrusive bodies that are Jurassic to Cretaceous in age. There are several significantly mineralized properties in the corridor between the Tintina and Denali faults. For example, the Coffee project (Fig. 1b) along the Tintina fault is a hydrothermal Au deposit with an indicated resource of 2.82 Moz ounces at 1.68 g/t Au and the Casino project (Fig. 1b) is a Au-Cu-Mo-porphyry deposit with an inferred resource of 9.0 Moz Au.
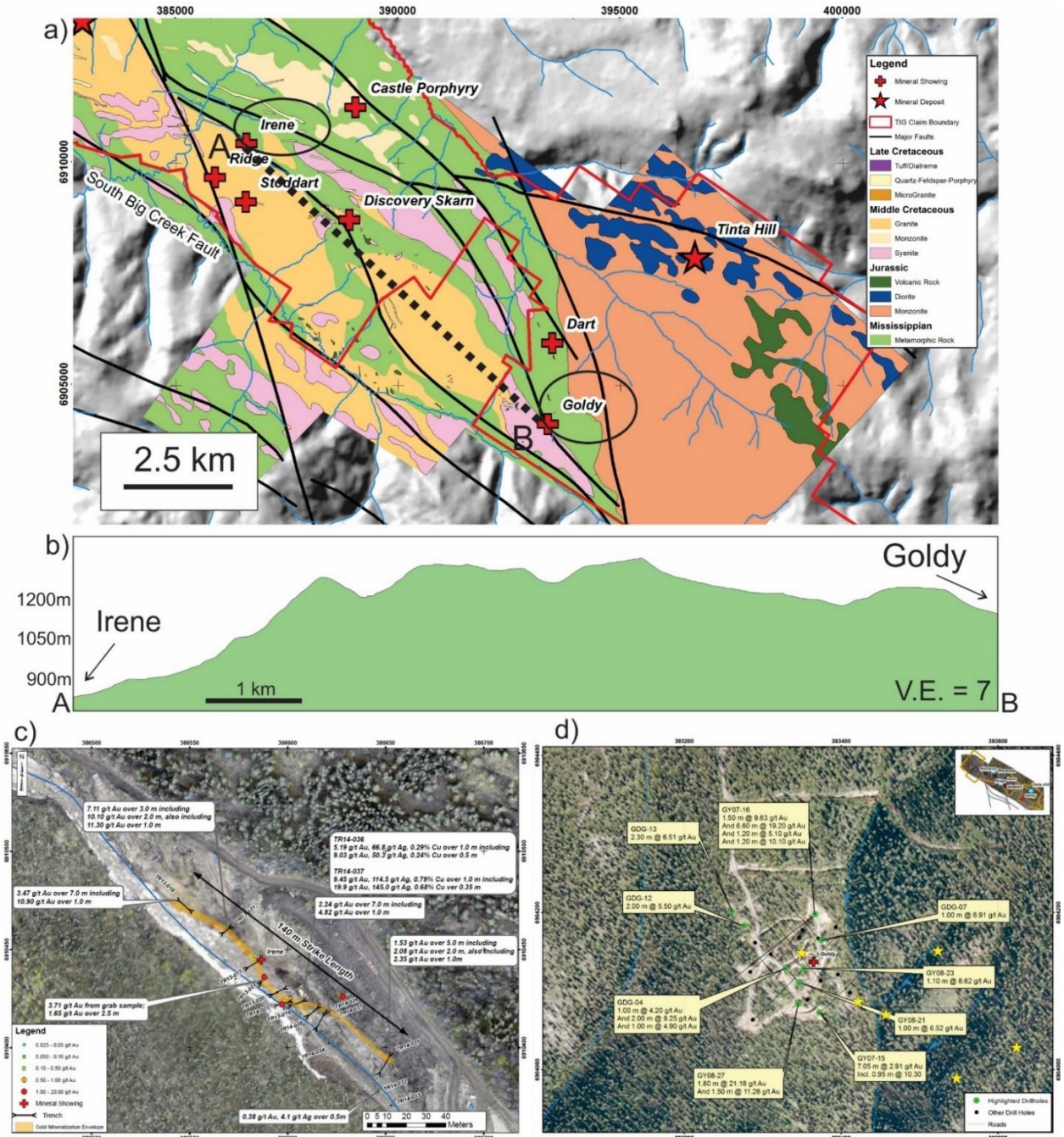
Figure 2. Location and geological setting of the Irene and Goldy showings at the Freegold Mountain property. (a) Plan view map of the study area at the Freegold Mountain property showing linear cross-section A-B trace between both showings shown in (b). (b) Cross-section A-B of the relative elevation between both showings. (c) Plan view map of Irene showing traces of the drill holes and their assay results. (d) Plan view map of Goldy with traces of drill holes and surface sample (stars) locations.

2.1.2 Goldy

The Goldy showing comprises a roughly 160 by 160 metre elliptical area (Fig. 2d) of quartz-stockwork veining. The predominant lithologies are quartz-biotite schist and granodiorite orthogneiss of the Yukon-Tanana terrane with Jurassic-age pluton intrusions of syenite and granodiorite of the Long Lake suite (Friend et al., 2018). There have been multiple hydrothermal events generating mm-size quartz-carbonate veins, "blue quartz" breccias which are >cm in size, and late chalcedonic quartz veins >cm in size (Fig. 4a). Historical drilling activities revealed several intersections that showed Au concentrations up to several g/t Au (Fig. 2d,3). High Au grades tend occur at hole intersections in "blue quartz" breccias and at lithological contacts as depicted in the down hole section of drill hole 07GY-16 (Fig. 3).
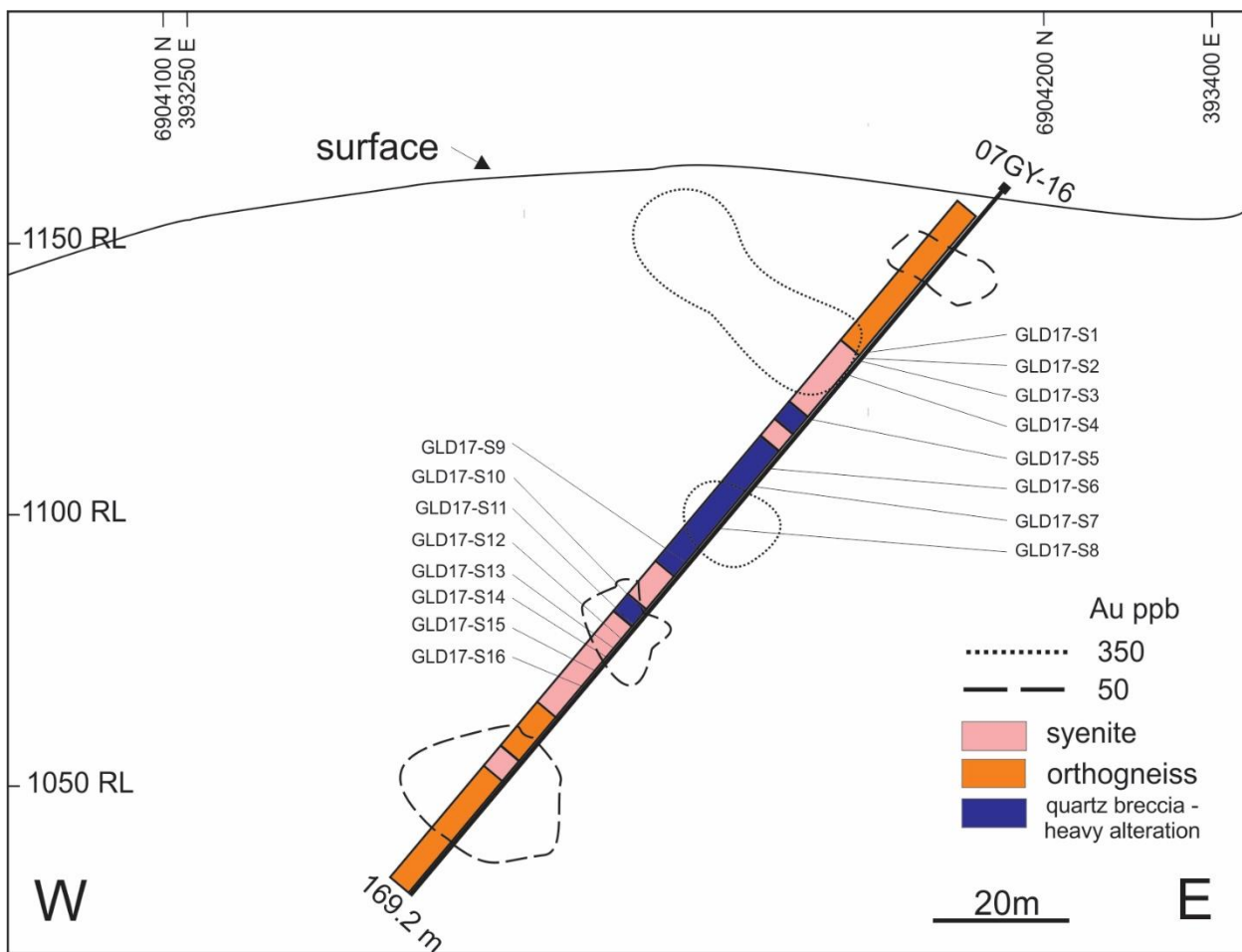
Figure 3. Cross-section from west to east taken from drill core 07GY-16 showing relative Au values and rock type. Visual of sample location depths, descriptions and bulk rock assay seen in Appendix 1 and Appendix 2a. Extrapolations of Au-grades are based on intersecting drill holes. Intervals of high Au-mineralization appear to occur in lithology changes and sections of heavy alteration from quartz brecciation. RL = relative elevation to sea level.

2.1.3 Irene

The Irene property contains a NW-trending gold bearing vein system that runs along Guder Creek (named after one of the regions pioneer prospectors in the 1930s) and extends approximately 150 meters in length, roughly 3 meters thick (Fig. 2c). Situated 9.5 km NW of Goldy property, the predominant lithologies at the Irene showing include Yukon-Tanana orthogneiss that is encountered throughout the region, and biotite-hornblende granodiorite to granite intrusions. At both showings roughly fault/contact-parallel quartz-feldspar-porphyry dykes are present and are interpreted to occur along segments or splays associated with the regionally important Big Creek Fault (Fig. 1).

3.0 Sampling and Analytical Methods

3.1 Sampling

Rock samples from the Goldy property were collected from both diamond drill core from the 2016 drilling program (DDH 07-GY-16) and from the Goldy property as chip samples from sub-crop (Fig. 2d and 3) or outcrop occurrences. Samples from the Irene showing were taken as chip samples or sub-crop or outcrop occurrences. For both properties, the goal was to collect a representative sample of outcrop rock types and mineralization styles.

3.2 Scanning Electron Microscopy - EDS – BSE

Quantitative and qualitative (identification only) analyses (energy dispersive spectroscopy – EDS) of gangue, ore, accessory minerals in the hydrothermal veins, and backscattered electron (BSE) imaging to characterize textures were performed using a TESCAN MIRA

3 LMU Variable Pressure Schottky Field Emission Scanning Electron Microscope (SEM) at Saint Mary's University, Halifax, Nova Scotia, Canada. The SEM is equipped with a back scattered electron detector coupled with energy dispersive spectrometer (EDS) functionality located at Saint Mary's University. For the latter, a solid state, 80 mm^2 X-max Oxford Instruments EDS detector was used. A beam voltage of 20 kV for an approximate working distance of 17 mm was used for all analysis.

3.3 Bulk rock assays

The results for the assayed samples (Appendix 2a and 2b) for both properties were taken from diamond drill core from the 2007 program on the Goldy property and 2018 on the Irene property.

Samples from the Goldy property were sent to EcoTech Laboratory in Kamloops, British Columbia for geochemical analysis of gold by 30g fire assay with an AA finish. Over limit (>1000 ppb Au) were reassayed and reanalyzed. Other elements were analyzed by four acid digestion and 24 element ICP-MS determination (Northern Freegold Resources Ltd., 2007).

The assay results for the Irene property were provided from the 2018 drilling program and samples were analyzed by SGS Canada of Vancouver, British Columbia. They were prepared for analysis according to SGS method PRP89: each sample was crushed to 75% passing 2 mm and a 250 g split was pulverized to better than 85% passing 75-micron mesh. Gold was tested by fire assay with atomic absorption finish on a 30g nominal sample (method GE FAA313), and samples that tested over 10 g/t Au were retested using a 30 g nominal sample and gravimetric analysis (method GO FAG303). An additional 35

elements were tested by ICP-AES using a four-acid digestion (method GE ICP40B) (Triumph Gold Corp, 2019).

3.4 Microthermometry

Microthermometric measurements on fluid inclusions were performed using a Linkam FTIR 600 heating-freezing stage mounted on an Olympus BX51 microscope at Saint Mary's University, Halifax, Nova Scotia. The stage was calibrated using synthetic fluid inclusion standards containing pure CO_2 (melting at $-$ 6.6°C) and pure, critical density H_2O (melting at 0°C and homogenizing at 374.1°C). Total uncertainties associated with the microthermometric measurements, based on the reproducibility of measurements conducted on the standards and the measurement precision of the instrumentation, range from ±2° to 3°C for temperatures recorded near the extremes of working conditions for the heating-freezing stages (–190° to 560°C), to less than ±0.2°C for temperatures recorded near 0°C. Final ice melting temperatures (T_m^{ice}) were used to calculate NaCl weight percent equivalency values for the inclusions (i.e., bulk salinity) based on the salinity-freezing point depression relationship of Bodnar and Vityk (1994).

3.4 Electron microprobe

Arsenopyrite (in equilibrium with pyrite) was analyzed for the purpose of constraining mineralization conditions using established thermobarometers, requiring quantitative WDS data. Analyses of the arsenopyrite were performed on a JEOL JXA8200 electron microprobe at Dalhousie University, Halifax, Nova Scotia, using a focused beam operating at an accelerating voltage of 15 kV, a beam current of 20 nA, and a spot size of 1 μm. Counting times for analyses were 10 s on each background and 20s on each

peak. Arsenopyrite analyzed for S, Fe, Zn, and As using in-house standards of pyrite (S), pyrrhotite (Po), sphalerite (Zn), and arsenopyrite (As) for calibration. These data were used in thermometry graphical estimations using the calibration of Kretschmar and Scott (1976).

4.0 Results

4.1 Bulk rock and statistical analysis

Bulk rock statistical analysis from assay results from the 2007 (Goldy) and 2018 (Irene) drilling campaigns show that Au has a significant positive (Pearson) correlation with As at the Goldy property (r=0.74) and a significant positive correlation with Sb (r=0.80) in the Irene property (Fig. 4a and 4b, Table 1 and 2). These associations are supported by petrographic and SEM-BSE images in the Irene samples of Au (as electrum) occurring in assemblages with the Sb-mineral stibnite, boulangerite, kobellite, sorbyite $[CuPb_9(Sb,As)_{11}S_{26}]$, and hakite $[Cu,Ag)_6Cu_4(Zn,Cu)_2(Sb,As)_4S_{13}]$. At the Goldy property the significant Au-As correlation cannot be supported by petrographic observations from the sample suite, as Au was never observed. However, high Au grades correlate with intervals of highly altered fragmental rock characterized by pervasive VG3-type quartz breccia, which is rich in arsenopyrite. These intervals show the presence of "blue quartz" as a potential visual indicator of Au grade in the field. This quartz breccia is present in both properties and appears to be related to a post ore-vein mineralization event. At the Irene showing, Au shows a correlation with As (r=0.55) indicating that Au is likely associated with arsenopyrite in the "blue quartz" breccias. The origin of the arsenopyrite, however, is unclear but its voluminous presence is noteworthy.
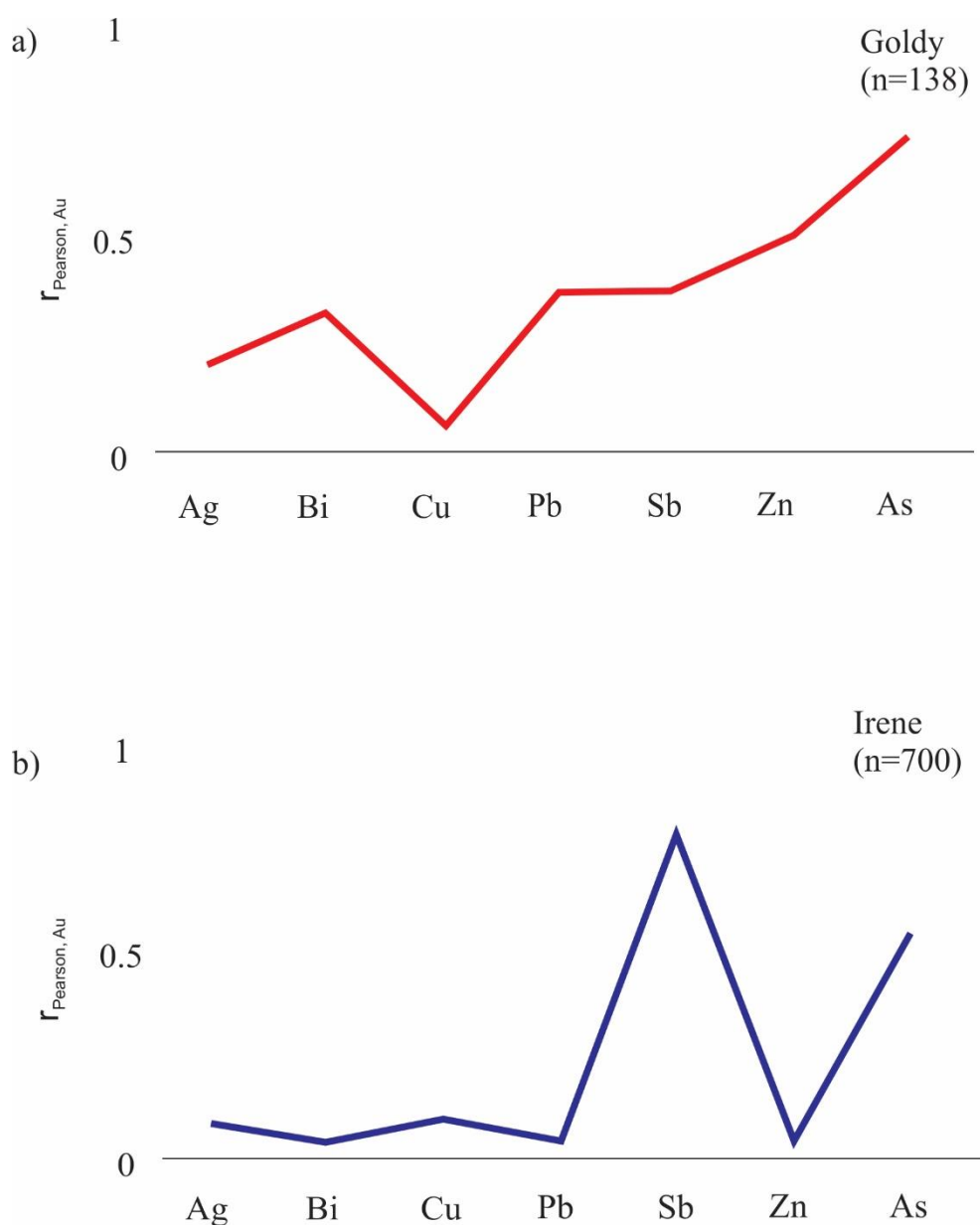
Figure 4. Bulk rock data from assay results analyzed for (Pearson) correlations between Au and other typical epithermal metals. (a) The Goldy property shows there is a significant correlation with As, n=138 assayed samples. (b) The Irene property shows a correlation with Sb with a n=700 assayed samples. Assay results can be seen in Appendix 2a and 2b.

Table 1. Pearson correlation coefficients for gold and other epithermal metals for the Goldy property

	Au	Ag	Bi	Cu	Pb	Sb	Zn	As
Au	1							
Ag	0.20374	1						
Bi	0.33053	-0.01149	1					
Cu	0.06548	0.15514	-0.05153	1				
Pb	0.37822	0.72330	0.10483	0.00307	1			
Sb	0.38192	0.61855	0.29004	0.10394	0.72829	1		
Zn	0.51652	0.50555	0.19147	-0.00448	0.83995	0.58937	1	
As	0.74441	0.46914	0.27687	-0.00634	0.69336	0.62503	0.77477	1

Notes: based on 138 assays

Table 2. Pearson correlation coefficients for gold and other epithermal metals for the Irene property

	Au	Ag	Bi	Cu	Pb	Sb	Zn	As
Au	1							
Ag	0.09966	1						
Bi	0.05135	0.62901	1					
Cu	0.11163	0.78222	0.45294	1				
Pb	0.05633	0.62725	0.1612	0.07867	1			
Sb	0.80386	0.03941	0.01444	0.04938	0.01455	1		
Zn	0.06126	0.46404	0.10896	0.24943	0.80961	0.00385	1	
As	0.55726	0.57256	0.42933	0.44137	0.32468	0.2704	0.32543	1

Notes: based on 700 assays

4.2 Vein Petrography and descriptions

4.2.1 Goldy

Vein types at the Goldy property (vein styles given identifier 'VG') have been classified from type 1 (earliest) through type 4 (latest) based on mineralogy and relative timing of emplacement observing through cross-cutting relationships (Fig. 5,9). All veins have apertures mm- to cm- wide. The earliest veins observed are classified here as VG1-type carbonate(dolomite)-pyrite-sphalerite-arsenopyrite with trace amounts of tetrahedrite-tennantite. Type VG2 veins are hydrothermal quartz-pyrite-chalcopyrite-sphalerite veins with subsidiary galena-rutile-boulangerite. The quartz shows euhedral crystal growth textures (Fig. 5c). Type VG3 veins are comprised of fine-grained dark blue quartz matrix, with brecciated host rock fragments that range from mm- to cm-size containing arsenopyrite with trace carbonate and barite fragments. Type VG4 veins are chalcedonic quartz veins with plumose margins containing no mineralization (Fig. 5a).
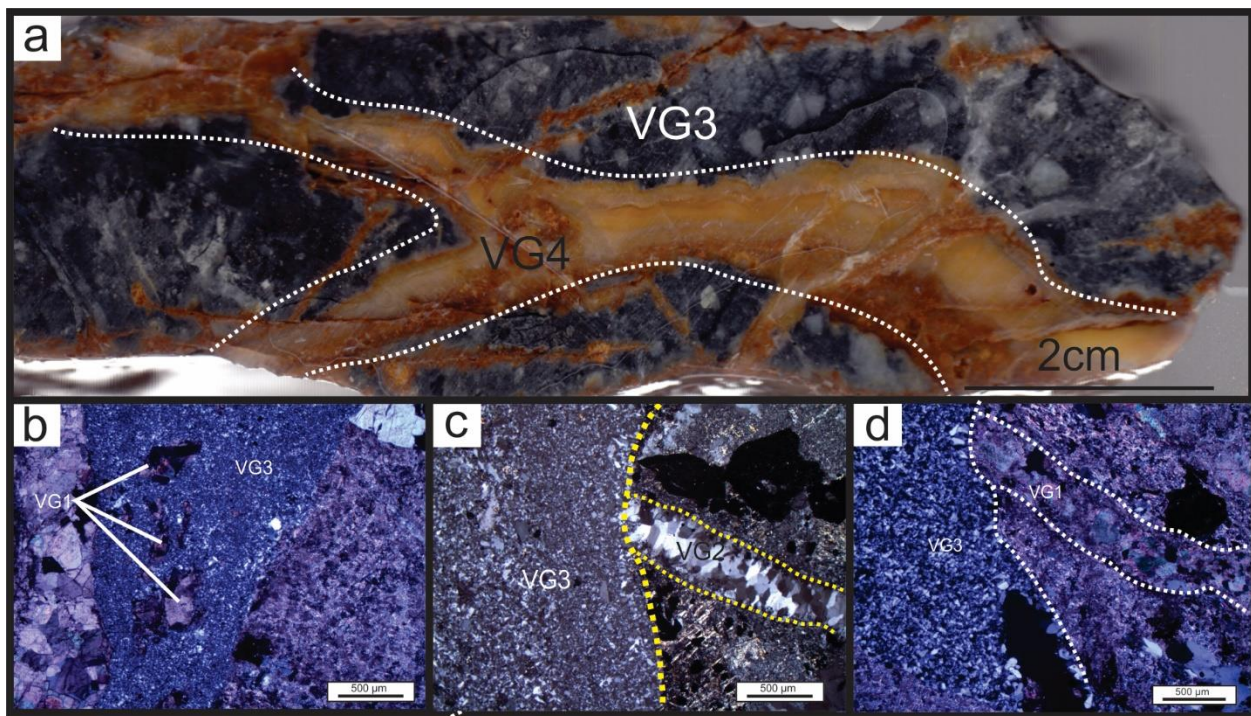
Figure 5. Goldy hand sample and thin section images showing hydrothermal vein types and cross-cutting relationships. (a) VG4-type chalcedonic quartz cross-cutting VG3-type quartz breccia. (b) VG3-type quartz cross-cutting and brecciating VG1-type carbonate veining. (c) VG3-type vein cross-cutting VG2-type hydrothermal quartz vein. (d) VG3-type vein cross-cutting VG1-type carbonate vein in sericitized host.

In VG1- and VG2-type veins pyrite is texturally and spatially associated with arsenopyrite (asp) as intergrowths and as a coating (Fig. 6c and f), sphalerite occurs as inclusions in galena, and galena occurs as both inclusions in pyrite and in textural equilibrium with pyrite (py) (Fig. 6a and c). Less commonly, tetrahedrite-tennantite is observed as fracture filling in pyrite (Fig. 6d), rutile occurs as a coating on arsenopyrite (Fig. 6 e and f), and boulangerite occurs as inclusions in galena associated with sphalerite (Fig. 6a).
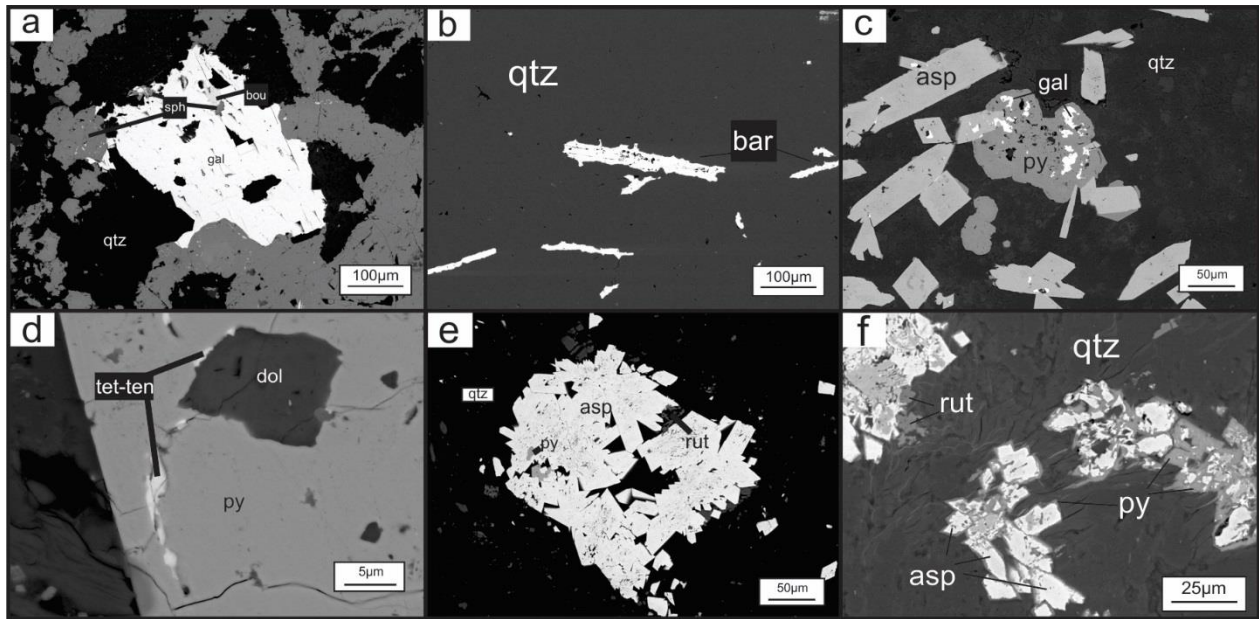
Figure 6. Scanning electron microscopy-backscattered electron (SEM-BSE) images from the Goldy property showing precious metal and accessory mineral assemblages in VG1/2-type mineralized veins for Goldy (a-f). (a) Galena (gal) grain with textural and spacial relationship with sphalerite (sph) and boulangerite (bou) inclusions. (b) Barite (bar) grains in V3-type quartz (qtz) breccia. (c) Pyrite (py) in textural relationship with arsenopyrite (asp) with galena (gal) inclusions. (d) Pyrite (py) grain with fracture filling dolomite (dol) and tetrahedrite-tennantite (tet-ten). (e-f) Arsenopyrite grains with with pyrite (py) inclusions and rimmed by rutile (rut) rimming.

4.2.2 Irene

Vein types at the Irene property have been classified as type 1 (earliest) through type 5 (latest) based on mineralogy and relative timing of emplacement observing through cross-cutting relationships (Fig. 7,9). All veins have mm- to cm-size aperture widths. The earliest veins observed are classified here as V1 type hydrothermal quartz-carbonate with trace to minor amounts of pyrite-arsenopyrite-stibnite-electrum. Veins are sub-mm width with jigsaw texture (Moncada, et al., 2012). Type V2 veins consist of Fe-carbonate with subsidiary pyrite-chalcopyrite-galena-barite-rutile. Type V3 veins is a fine grain dark blue brecciating quartz that range from mm- to cm-size containing arsenopyrite with trace barite-sphalerite-tetrahedrite-tennantite. This vein type continually assays high gold (Fig. 4b). Type V4 veins are a late stage hematite that has been observed in an anomalous sulfide-rich sample that is thought to be a high-grade shoot of the system. Type V5 veins are wispy sub-mm size carbonate vein that is not mineralized.
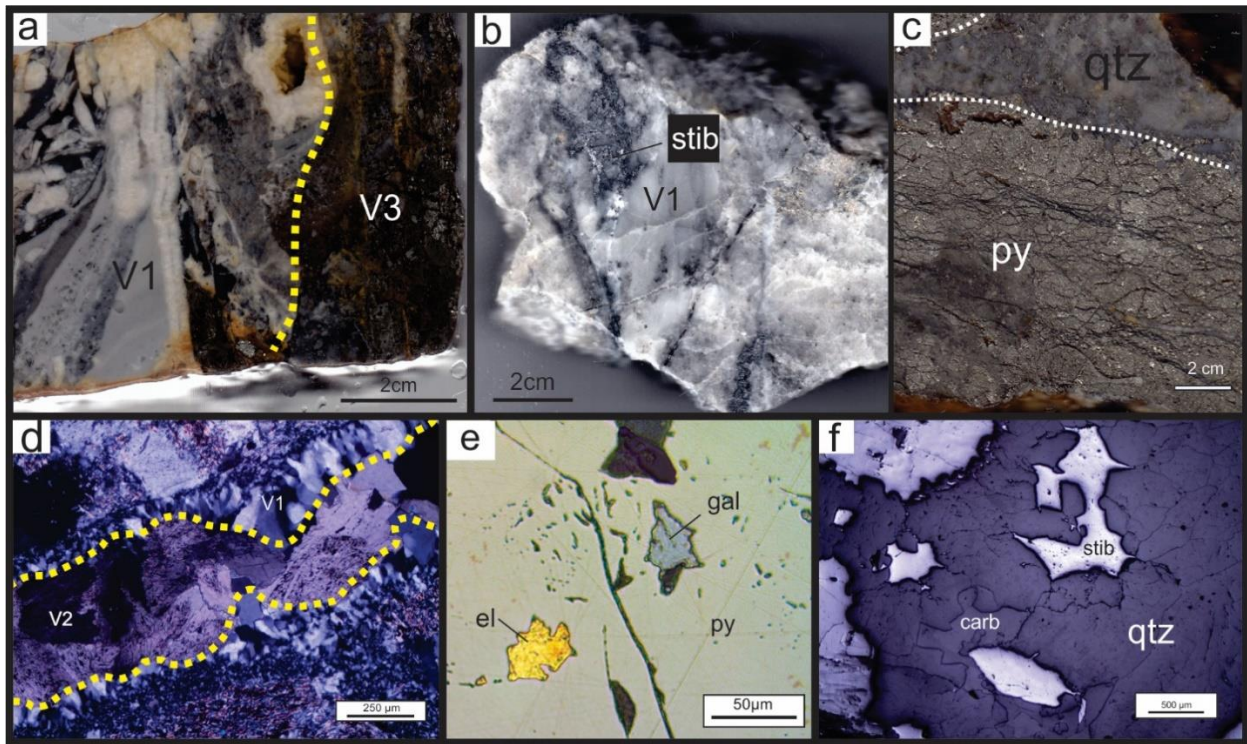
Figure 7. Irene hand sample and thin section images showing hydrothermal vein types and cross-cutting relationships. (a) V1-type quartz-carbonate vein relationship with V3-type quartz breccia vein. (b) V1-type quartz-carbonate-(stib) stibnite vein in granitoid host. (c) massive sulfide primarily composed of py(pyrite) with a cross-cutting qtz(quartz) vein. (d) V2-type Fe-carbonate hydrothermal vein laminating V1-type vein. (e) el(electrum) and (gal)galena inclusions in pyrite grain. (f) stib(stibnite) mineralization in V1-type (qtz)quartz

Within V1 and V2 veins, electrum, Sb-minerals, galena, and tetrahedrite-tennantite occur as inclusions in pyrite (Fig 8c, e and f). Stibnite mineralization occurs as either cavity infillings (Fig. 8a) or in textural equilibrium with quartz-carbonate grains with cuspate margins (Fig. 7f) potentially indicating a volume change. Their relative timing of precipitation in relation to other major sulfide and gangue phases is summarized in Fig. 9. Cross-cutting relationships between these two veins demonstrates that there were two phases of metallic mineralization (Fig. 7h). Type V2 veins mineralize stibnite with textural relationship with boulangerite.
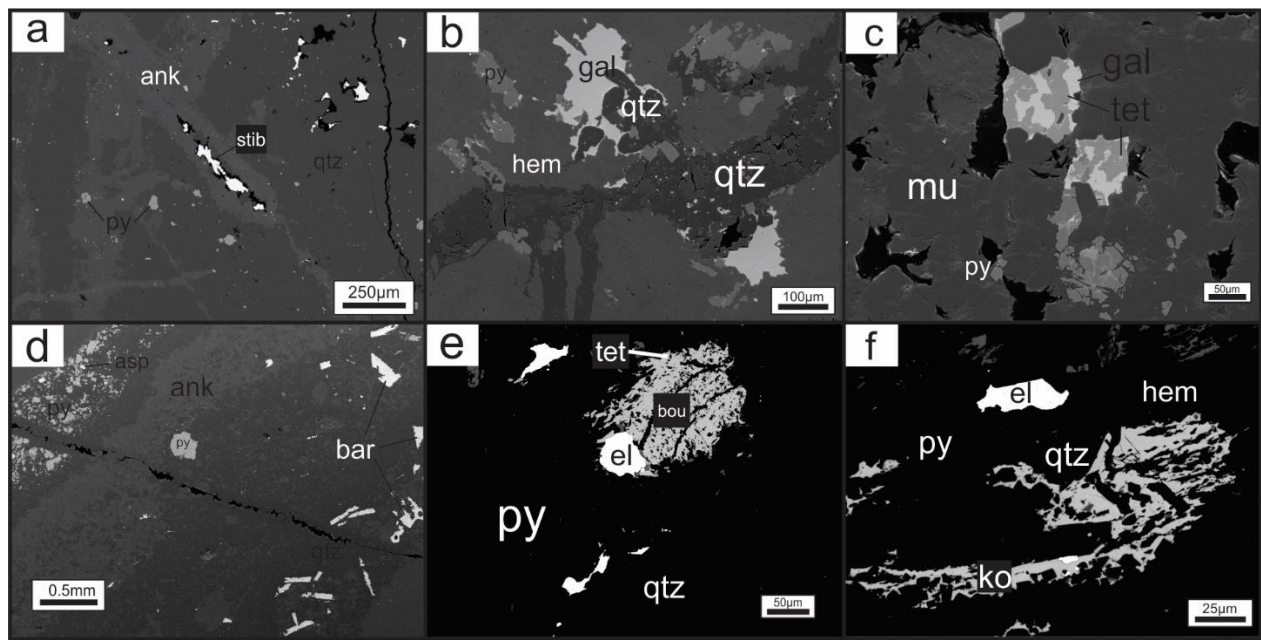
Figure 8. Scanning electron microscopy-backscattered electron (SEM-BSE) images from the Irene property**.** (a) Stibnite (stib) mineralization in ankeritic V1-type vein. (b) Quartz (qtz) veining with late galena (gal) mineralization. (c) Textural relationship between galena and tetrahedrite-tennantite (tet-ten). (d) Barite (bar) mineralization in quartz breccia V3-type vein similar to image (Fig. 6b). (e) Boulangerite (bou) mineralization occuring with electrum (el) (~90% Au, 10% Ag;Table 1) (f) Kobellite (kob) [$Pb_2(Bi,Sb)_2S_5$] mineralization in spacial relationship with electrum in V1-type vein.
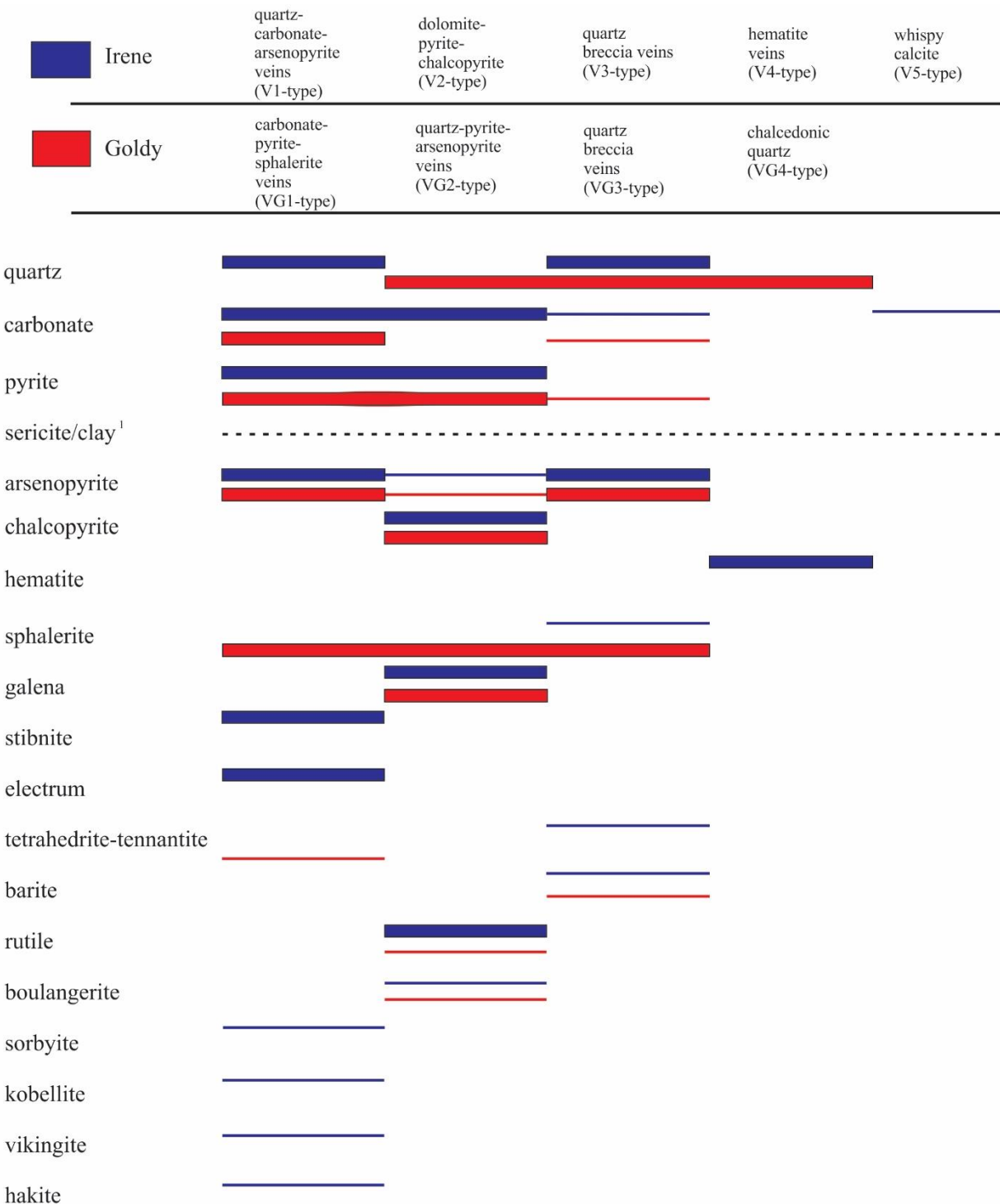
Figure 9. Paragenetic sequence and relative abundance of minerals in intermediate epithermal deposit precipitated. Thick lines represent the stages of major mineral phase deposition; thin lines represent minor or trace mineral deposition.

Table 3 Representative analysis (SEM-EDS) of precious metal minerals and other accessory minerals in vein stages 1 and 2

Analysis no.	1	2	3	4	5*	6	7	8*	9	10*	11	12	13	14	15	16	17
Ag (wt%)	10.7	13.3	28.4	-	3.1	-	4.7	-	-	-	-	-	-	-	9.8	-	-
As	-	-	-	2.1	4.8	6.1	2.0	-	-	6.9	-	-	-	-	-	7.3	8.5
Au	89.3	83.9	71.6	-	-	-	-	-	-	-	-	-	-	-	-	-	-
Bi	-	-	-	-	-	-	-	-	-	-	-	-	-	-	49.5	-	-
Cu	-	-	-	35.3	27.3	32.8	32.4	-	-	13.3	-	-	12.4	10.8	-	30.3	35.2
Fe	-	0.7	-	2.3	10.1	1.4	3.8	-	-	-	-	-	-	-	-	6.5	6.5
O	-	2.2	-	-	-	-	-	-	-	-	-	-	-	-	-	-	-
Pb	-	-	-	-	-	-	-	52.7	49.8	42.7	-	-	38.7	39.7	23.3	-	-
S	-	-	-	27.1	33.3	29.7	27.8	20.4	22.3	21.6	28.8	28.7	23.9	22.6	17.3	32.4	30.5
Sb	-	-	-	28.5	15.8	23.7	26.3	26.9	27.9	15.5	71.2	71.3	25.0	27.0	-	23.5	19.3
Zn	-	-	-	4.2	5.5	6.0	3.1	-	-	-	-	-	-	-	-	-	-
Total	100.0	100.0	100.0	100.0	100.0	100.0	100.0	100.0	100.0	100.0	100.0	100.0	100.0	100.0	100.0	100.0	100.0

Notes: dashes indicate elements not detected, mineral key:1-3 = electrum, 4-7 = tetrahedrite-tennantite, 8-9 = boulangerite, 10 = sorbyite, 11-12 = stibnite, 13-14 = kobellite, 15 = vikingite, 16-17 = hakite. * indicate minerals seen in Goldy samples. Analysis no. 1,2,3,4,6,7,9,11,12,13,14,15, and 16 are found in Irene samples.

4.3 Arsenopyrite thermometry

To obtain an independent estimate of vein formation temperature, the atomic % As content of arsenopyrite in textural equilibrium with pyrite was determined using an electron microprobe. Using the thermometer of Kretschmar and Scott (1976). Crystallization temperature for arsenopyrite at the Irene showing ranged from 382-432°C and (30-32 As atomic %) whereas crystallization temperature for arsenopyrite at the Goldy showing showed two generations of arsenopyrite-pyrite mineralization with temperature constraints between 300-346°C and 393-427°C, corresponding to As atomic % ranges of 29-30 and 31-32%, respectively. Overlapping compositional-T fields suggests that arsenopyrite-pyrite mineralization at both properties formed at similar conditions (Fig. 10 and Table 3).

Although there is only 1 (one) observed sample of sphalerite-arsenopyrite in textural equilibrium recorded (Goldy property), the Zn% composition is consistent with the low-temp sphalerite analysis with Fe (Scott, 1983).
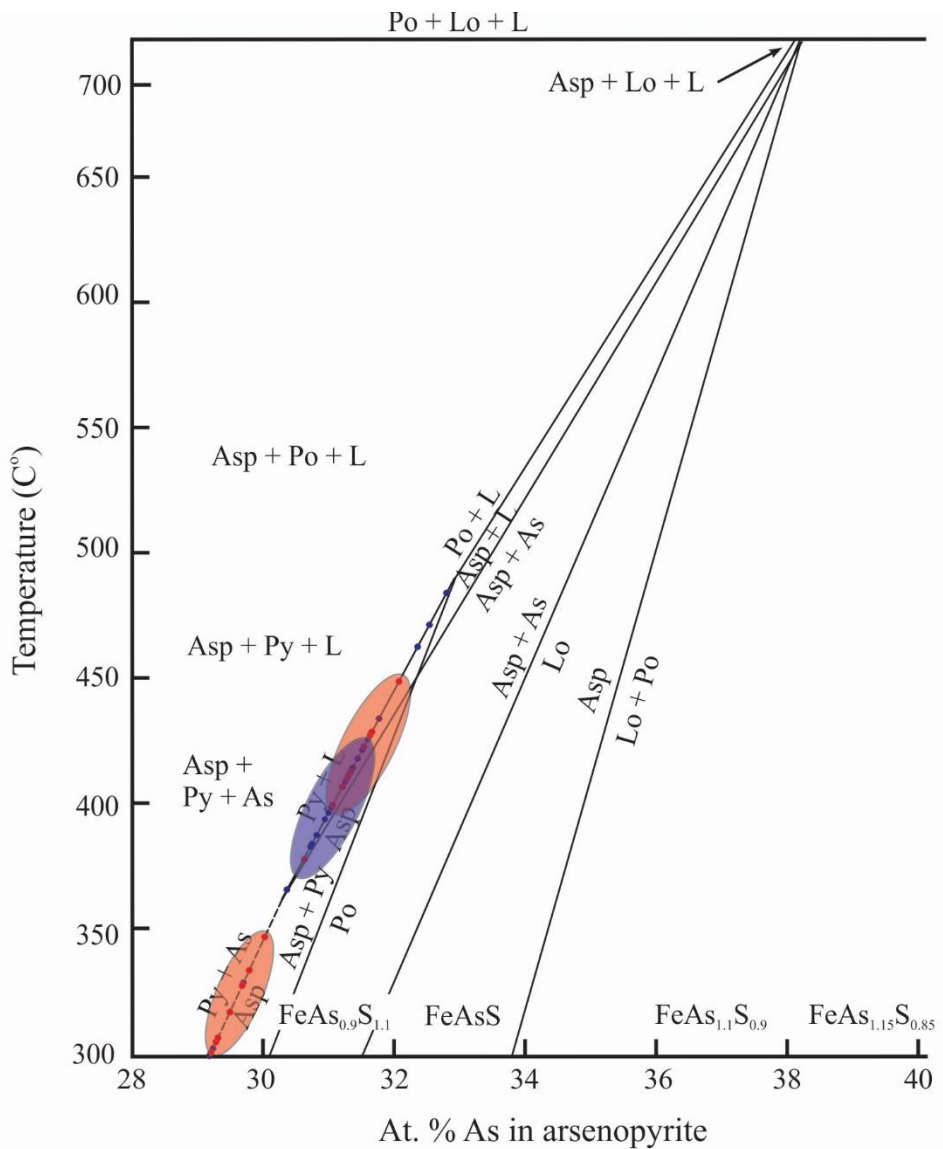
Figure 10. Electron microprobe analysis of arsenic in arsenopyrite shown on a T-X diagram. Electron microprobe analysis of atomic % As in the arsenopyrite-pyrite assemblage indicates a constrained temperature parameter for the Goldy (red) and Irene (blue) mineralization. Showing two arsenopyrite-pyrite mineralization phases between 300-346°C and 393-427°C for the Goldy property and Irene at 382-432°C. Asp – arsenopyrite, L = liquid, Po = pyrrhotite, Py = pyrite, As = arsenic, Lo = löellingite, S = sulfur. Image modified from Kretschmar and Scott (1976).

Table 4 Electron microprobe data for Irene and Goldy

| Sample no. | | Wt% | | | | Atomic% | | | | |
		Fe	S	As	Zn	Fe	S	As	Zn	Total
IR17-S-S5	asp	34.77	21.34	45.14	-	32.95	35.22	31.89	-	100.00
IR17-S-S5	asp	35.00	21.33	44.75	-	33.18	35.22	31.63	-	100.00
IR17-S-S5	asp	34.99	20.80	45.62	-	33.26	34.43	32.32	-	100.00
IR17-S-S5	asp	35.29	22.36	40.76	-	33.73	37.22	29.03	-	100.00
IR17-S-S5	asp	34.90	20.90	45.62	-	33.14	34.58	32.29	-	100.00
IR17-S-S5	asp	34.83	21.35	44.28	-	33.16	35.40	31.42	-	100.00
IR17-S-S5	asp	34.74	22.28	41.61	-	33.22	37.10	29.65	-	100.00
IR17-S-S5	asp	35.18	22.60	41.10	-	33.45	37.42	29.13	-	100.00
GLD17-S10	asp	35.74	24.11	43.40	-	32.31	37.97	29.25	-	100.00
GLD17-S10	asp	35.62	23.45	42.72	-	32.71	37.49	29.23	-	100.00
GLD17-S12	asp	35.79	22.83	42.42	-	33.38	37.09	29.49	-	100.00
GLD17-S12	asp	35.53	22.78	42.71	-	33.19	37.06	29.74	-	100.00
GLD17-S12	asp	35.57	22.77	42.90	-	33.18	37.00	29.83	-	100.00
GLD17-S12	asp	35.35	23.12	41.87	-	33.05	37.65	29.17	-	100.00
GLD17-S12	asp	36.16	24.66	39.86	-	33.21	39.45	27.29	-	100.00
GLD17-S12	asp	35.02	22.66	43.00	-	32.84	37.00	30.06	-	100.00
GLD17-S12	asp	35.23	21.79	44.58	-	33.12	35.66	31.23	-	100.00
GLD17-S12	asp	35.21	22.02	44.93	-	32.90	35.83	31.29	-	100.00
GLD17-S12	asp	35.13	22.10	44.75	-	32.85	35.99	31.19	-	100.00
GLD17-S14	asp	35.26	21.89	44.48	-	33.10	35.78	31.12	-	100.00
GLD17-S14	asp	35.74	23.96	41.23	-	33.05	38.58	28.41	-	100.00
GLD17-S14	asp	35.11	22.02	43.65	-	33.12	36.17	30.69	-	100.00
GLD17-S14	asp	34.93	20.96	45.28	-	33.20	34.70	32.09	-	100.00
GLD17-S10	sph	2.46	34.07	0.10	61.38	2.15	51.91	0.06	45.87	100.00
GLD17-S10	sph	2.52	34.16	0.12	61.90	2.19	51.74	0.08	45.99	100.00

Notes: Although there is only 1 (one) observed sample of sphalerite-arsenopyrite recorded the sphalerite composition in equilibrium with arsenopyrite is consistant with the low-temp sphalerite analysis with iron (Scott, 1983). asp = arsenopyrite, sph = sphalerite

4.4 Fluid inclusion petrography and microthermometry

Classification of fluid inclusion origin using formalized criteria from Goldstein (2003) was based on petrographic observations at room temperature. All fluid inclusions studied were hosted in quartz. Inclusions were concluded to be of the same assemblage if they were in the same trail or cluster, while similar homogenization temperatures and salinities were used to support criteria for assemblages. None of the studied inclusions were considered to be primary inclusions (occurring unambiguously along growth zones) and thus were either deemed of secondary "s" or unknown "u" origin.

4.4.1 Goldy

Two types of petrographically distinct fluid inclusion types were observed in Goldy quartz grains. Type-I and type-II inclusion assemblages consists of simple two-phase aqueous (liquid + vapor, at 20°C). Type-I inclusions were considered to be secondary and occur in trails that follow healed fractures and cross-cut grain boundaries (Fig. 11a and c). Type-II inclusions occur also in secondary trails. However, they did not provide microthermometric results due to inclusions being too small to measure at the optical resolution of the microscope set-up (size ~3 μm). Type-I inclusions range in size from 5 μm to 10 μm. All inclusions homogenized ($T_h^{L+V \to L}$) to a liquid phase by shrinking and disappearance of the vapor bubble (L+V$\to$L) from 178.9° to 247.7°C. Final ice melting temperature (T_m^{ice}) were observed to vary as well (with the exception of an anomalous -12.6°C measurement) between -6.6° and -0.2°C, corresponding to bulk salinities varying from 0.7 to 16.4 wt% NaCl eq. Single inclusion assemblages showed much narrower ranges in $T_h^{L+V \to L}$ and salinity. Data are summarized in Table 5.

4.4.2 Irene

All fluid inclusions observed in the Irene samples were either one-phase aqueous (liquid, at 20°C) or two-phase aqueous (liquid + vapor, at 20°C). Figure 11 show representative inclusions of the two varieties in photomicrographs. Type-I inclusions occur in planar arrays (trails) that cross-cut grain boundaries (Fig. 11d). These were considered to be secondary inclusions due to their occurrence along healed fracture surfaces. Type-II inclusions are in general larger in size than type-I and are less abundant. Their origin is unknown. All fluid inclusions ranged in diameter from 5 μm to 10 μm.

Microthermometric measurements (summarized in Table 5) were conducted on type-I inclusions and show a wide range of homogenization temperatures ($T_h^{L+V\rightarrow L}$) but a relatively narrow range of final ice melting (T_m^{ice}) temperatures. All inclusions homogenized to a liquid phase by shrinking and disappearance of the vapor bubble (L+V→L) over a range from 130.3° to 232.5°C. With exception of two outliers (-20.5 and -19.7°C), the T_m^{ice} ranged from -12.5° to -1.7°C, corresponding to bulk salinities varying from 2.9 to 22.7 wt% NaCl eq. Single inclusion assemblages showed much narrower ranges in $T_h^{L+V\rightarrow L}$ and salinity.
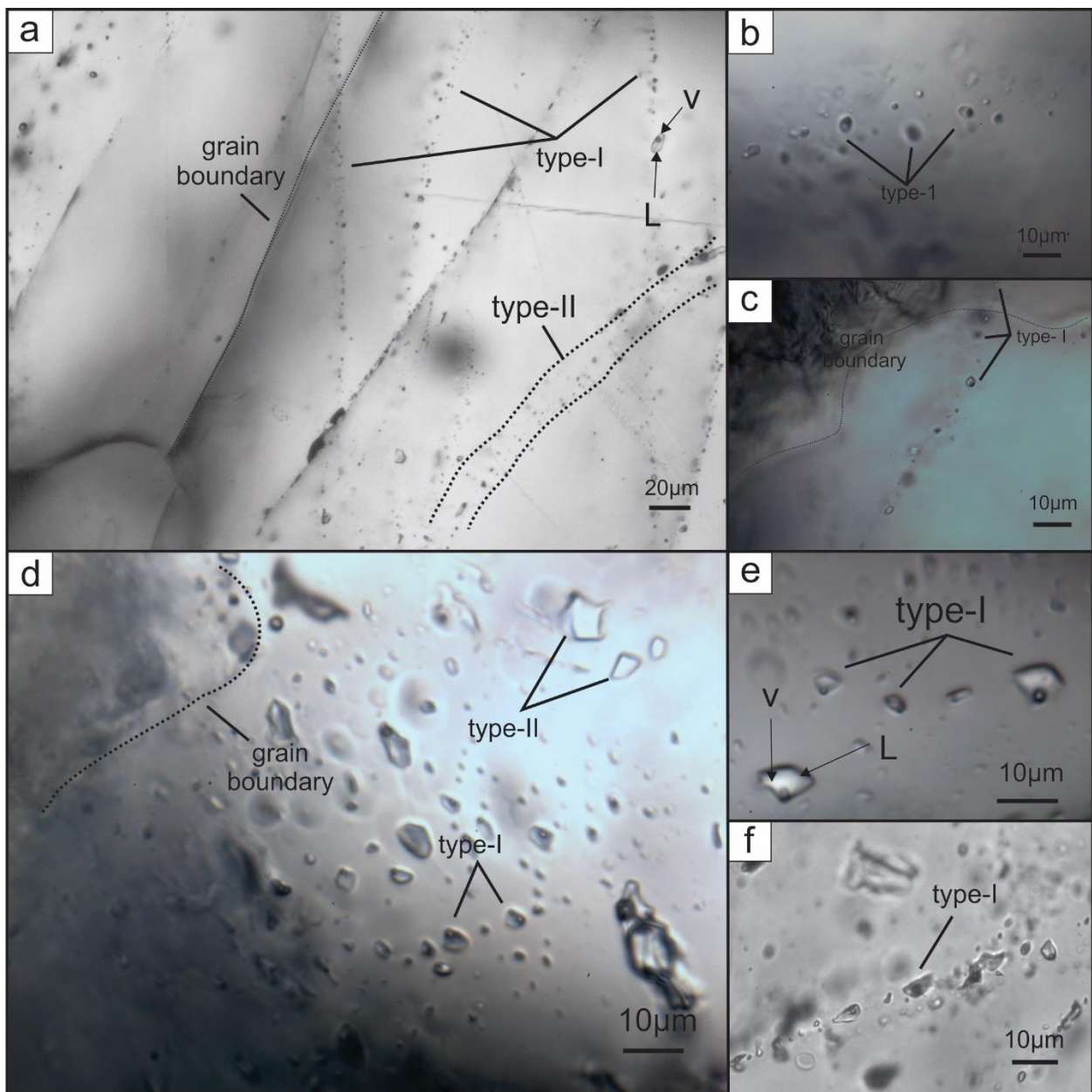
Figure 11. Transmitted light photomicrographs of type-I and type-II two-phase quartz-hosted fluid inclusions found on the Goldy and Irene properties. (a) Goldy type-I inclusions are secondary, fracture hosted, and cross cut grain boundaries. Type-II have an unknown origin and generally very small (~3 µm in size) and difficult to obtain measurements from. (b) Goldy two-phase (liquid and vapor) type-I inclusions. (c) Goldy type-I inclusions shown cross-cutting quarts grain boundary. (d) Irene planar array of mixed (heterogeneously trapped) aqueous type-I inclusions and single-phase type-II inclusions at. (e) Irene type-I inclusions. (f) Irene type-I inclusion trail. All images taken at room T, using 100x objective and a 10x eyepiece (~1000x magnification).

35
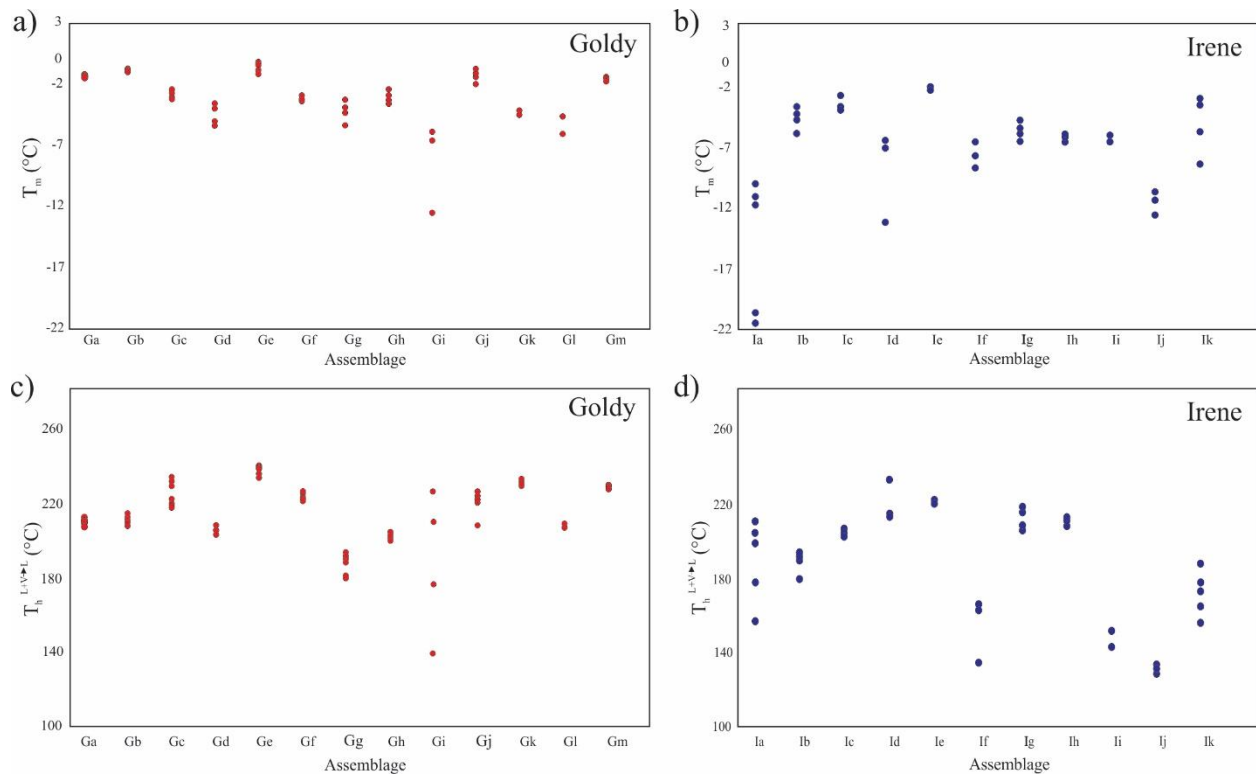
Figure 12. Final ice melting and homogenization temperatures of FIAs in quartz-hosted fluid inclusions. 51 inclusions were measured from Goldy and 40 from Irene. Final ice melting (T_m) temperatures on the y-axis record the complete melting of FIAs in quartz fluid inclusions. a) shows the range in melting temperatures between -12.6 and -0.2°C. b) shows the temperature range for Irene between -20.5 and -1.7°C. Graphs c and d show the homogenization ($T_h^{L+V \to L}$) of properties Goldy and Irene and the temperatures on the y-axis give the point at which the two-phase (liquid and vapor) fluid transitioned into a single-phase fluid. c) Demonstrates the range of $T_h^{L+V \to L}$ for Goldy assemblages between 178.9° – 247.7°C. d) demonstrates the range of $T_h^{L+V \to L}$ for the Irene assemblages between 130.3° to 232.5°C.
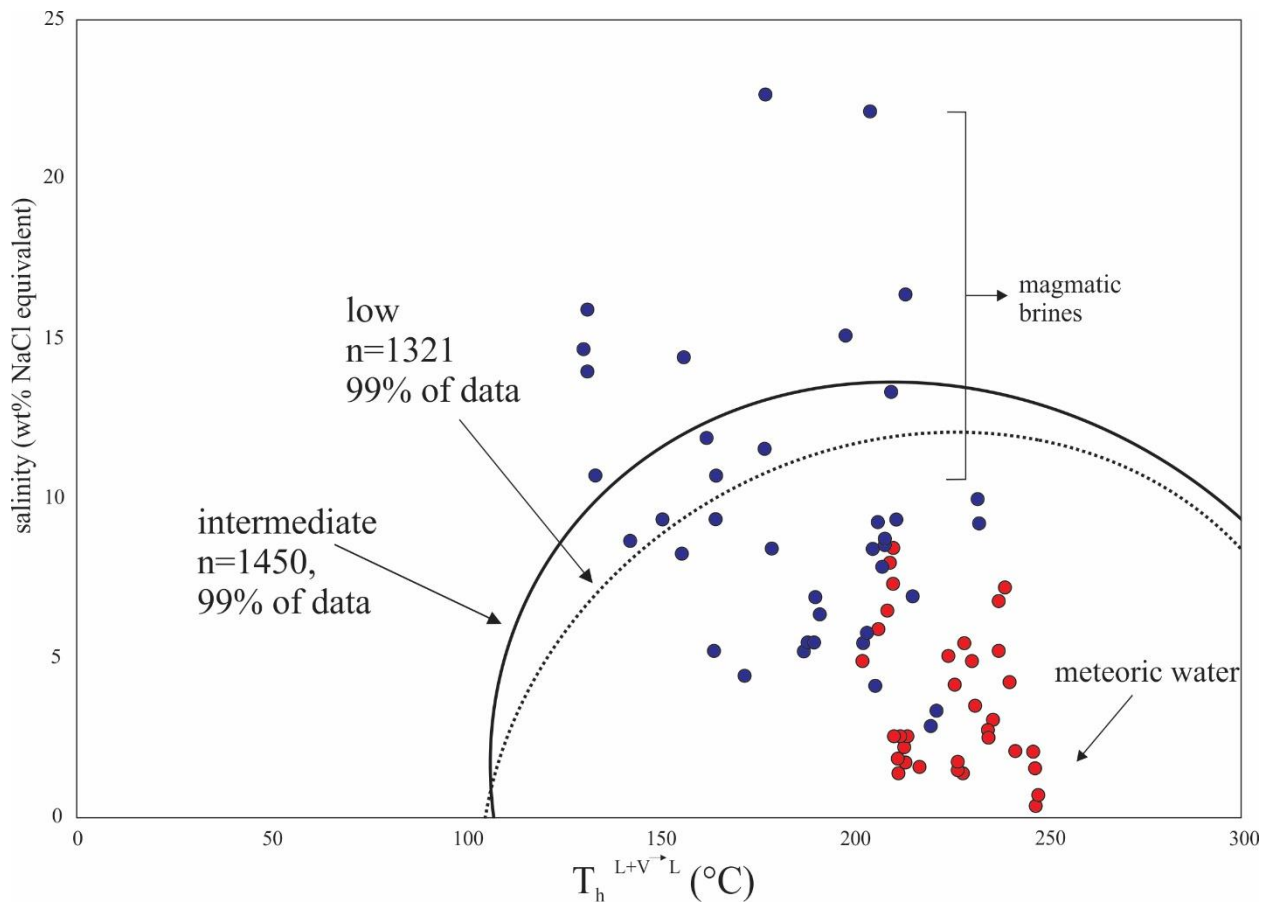
Figure 13. Plot of homogenization temperature ($T_h^{L+V \rightarrow L}$) vs. salinity (wt% NaCl equiv) showing data for all fluid inclusions measured in Irene (blue) n=40 and Goldy (red) n=51 hosted in quartz grains. The Goldy inclusions have a lower salinity and fall within the low-sulfidation field which form a continuous trend towards the more saline Irene inclusion fluids with a trend to the intermediate sulfidation field. The dashed and solid ovoid fields represent the window of low sulfidation and intermediate sulfidation ranges of homogenization temperature vs. salinity taken from Bodnar et al. (2014) where low-sulfidation deposits show $T_h^{L+V \rightarrow L}$ ranges of 105 to 360°C and salinities of 0 to 12 wt% and intermediate-sulfidation deposits show $T_h^{L+V \rightarrow L}$ ranges of 110 to 380°C with salinities 0 to 14 wt%.
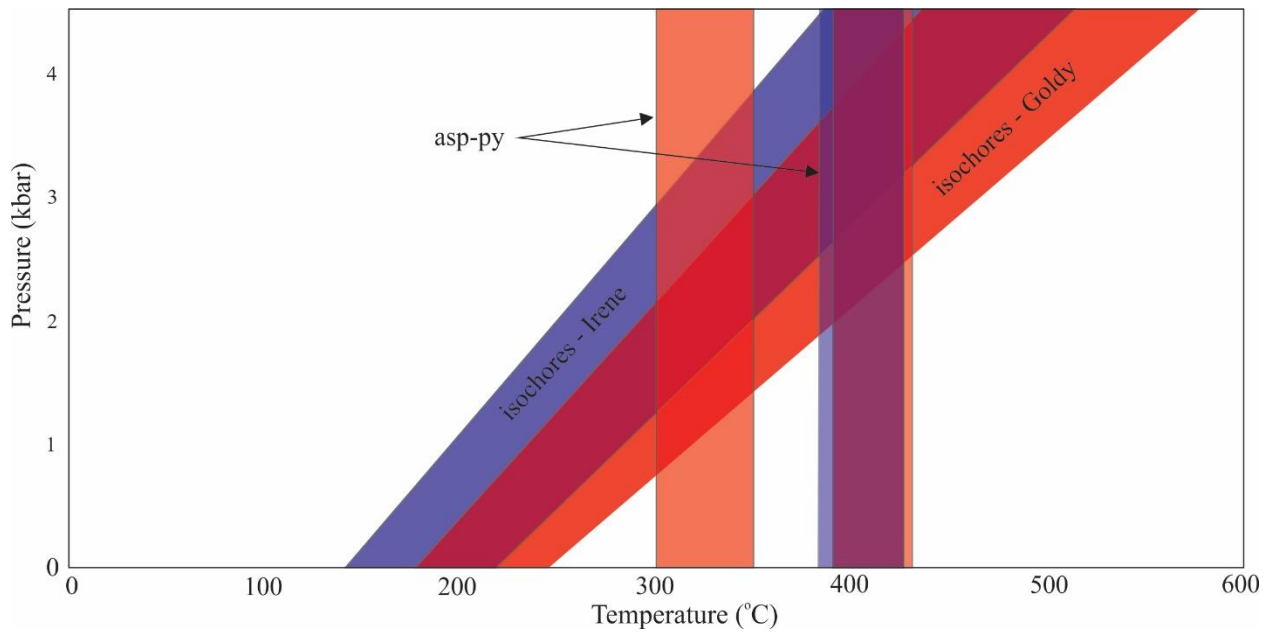
Figure 14. Fluid inclusion isochore ranges for the Goldy and Irene systems showing overlapping T fields from arsenopyrite-pyrite thermometry. The blue zone transitioning to the rightward extent of the diagonal purple zone represents the range of Irene fluid inclusion isochore data and the red zone transitioning to the leftward extent of the horizontal purple zone represents the Goldy fluid inclusion isochore data. The horizontal purple zone is the overlap between them. The vertical fields are the temperature constraints estimated from the arsenopyrite-pyrite microprobe results. The vertical purple field is the shared temperature regime of arsenopyrite generation for both properties.

Table 5. Fluid inclusion microthermometry data

Sample	A#	T_m^{ice} (°C)	$T_h^{L+V \rightarrow L}$ (°C)	S wt% NaCl eq	size (μm)	origin (s,p,u)	Sample	A#	T_m^{ice} (°C)	$T_h^{L+V \rightarrow L}$ (°C)	S wt% NaCl eq	size (μm)	origin (s,p,u)
Goldy 17-S-S5	Ga 2	-1.3	213.3	2.2	7	s	17-S-15	Gl 2	-4.6	210.5	7.3	-	s
17-S-S5	Ga 3	-1.5	214.2	2.5	6	s	17-S-15	Gm 1	-1.5	234.8	2.5	-	s
17-S-S5	Ga 4	-1.5	212.1	2.5	8	s	17-S-15	Gm 2	-1.6	234.9	2.7	-	s
17-S-S5	Gb 1	-0.8	211.7	1.4	-	s	17-S-15	Gm 3	-1.6	234.6	2.7	-	s
17-S-S5	Gb 2	-0.9	217.0	1.5	-	s	17-S-15	Gm 4	-1.8	236.0	3.0	-	s
17-S-S5	Gb 3	-1.0	213.5	1.7	-	s	Irene 17-S8	Ia 1	-10.4	156.5	14.4	-	s
17-S-S5	Gc 1	-2.6	240.4	4.3	-	s	17-S8	Ia 2	-19.7	204.1	22.2	-	s
17-S-S5	Gc 2	-3.1	237.4	5.2	-	s	17-S8	Ia 3	-9.4	209.5	13.3	-	s
17-S-S5	Gc 3	-2.5	226.2	4.1	-	s	17-S8	Ia 4	-11.1	198.0	15.1	-	s
17-S-S5	Gc 4	-3.0	-	4.9	-	s	17-S8	Ia 5	-20.5	177.1	22.7	-	s
17-S-S5	Gc 5	-3.1	224.4	5.0	-	s	17-S8	Ib 1	-5.4	178.9	8.4	9	s
17-S-S5	Gd 1	-5.4	210.3	8.4	5	u	17-S8	Ib 2	-3.3	188.8	5.5	6	s
17-S-S5	Gd 2	-5.1	209.6	8.0	5	u	17-S8	Ib 3	-3.9	191.6	6.4	10	s
17-S-S5	Gd 3	-3.6	206.7	5.9	6	u	17-S8	Ib 4	-3.3	190.1	5.5	10	s
17-S-S5	Gd 4	-4.0	208.9	6.5	7	u	17-S8	Ib 5	-4.3	190.3	6.9	8	s
17-S-S5	Ge 1	-1.2	241.9	2.0	7	s	17-S8	Ic 1	-3.5	204.0	5.8	10	s
17-S-S5	Ge 2	-1.2	246.3	2.0	5	s	17-S8	Ic 2	-2.5	205.8	4.1	6	s
17-S-S5	Ge 3	-0.9	247.0	1.5	6	s	17-S8	Ic 3	-3.3	202.6	5.5	5	s
17-S-S5	Ge 4	-0.4	247.7	0.7	5	s	17-S8	Ic 4	-6.0	232.5	9.2	8	s
17-S-S5	Ge 5	-0.2	247.0	0.3	4	s	17-S8	Id 1	-12.5	213.5	16.4	10	u
17-S-15	Gf 1	-3.0	231.0	4.9	5	u	17-S8	Id 2	-6.6	232.1	10.0	7	u
17-S-15	Gf 2	-3.3	228.6	5.5	5	u	17-S8	Ie 1	-2.0	221.3	3.3	-	s
17-S-15	Gf 3	-3.3	228.8	5.5	6	u	17-S8	Ie 2	-1.7	219.8	2.9	-	s
17-S-15	Gg 1	-5.4	178.9	8.4	11	s	17-S8	Ie 3	-1.7	219.8	2.9	5	s
17-S-15	Gg 2	-3.3	188.8	5.5	5	s	17-S8	If 1	-8.2	162.2	11.9	5	s
17-S-15	Gg 3	-3.9	191.6	6.4	10	s	17-S8	If 2	-6.1	164.5	9.3	7	s
17-S-15	Gg 4	-3.3	190.1	5.5	8	s	17-S8	If 3	-7.2	133.7	10.7	5	s
17-S-15	Gg 5	-4.3	190.3	6.9	7	s	17-S8	If 4	-7.2	164.5	10.7	8	s
17-S-15	Gh 1	-3.5	204.0	5.8	10	s	17-S8	Ig 1	-6.0	206.3	9.2	9	s
17-S-15	Gh 2	-2.5	205.8	4.1	8	s	17-S8	Ig 2	-5.4	205.2	8.4	8	s
17-S-15	Gh 3	-3.3	202.6	5.5	4	s	17-S8	Ig 3	-5.0	207.8	7.9	9	s
17-S-15	Gh 4	-3.0	202.4	4.9	4	s	17-S8	Ig 4	-4.3	215.3	6.9	6	s
17-S-15	Gi 1	-6.0	232.5	9.2	9	s	17-S8	Ih 1	-5.6	208.2	8.7	10	u
17-S-15	Gi 2	-12.5	213.5	16.4	6	s	17-S8	Ih 2	-6.1	211.2	9.3	8	u
17-S-15	Gi 3	-6.6	130.3	10.0	5	s	17-S8	Ih 3	-5.5	208.2	8.6	7	u
17-S-15	Gj 1	-1.5	210.8	2.5	8	s	17-S8	Ii 1	-6.1	150.8	9.3	8	s
17-S-15	Gj 2	-1.1	211.4	1.9	5	s	17-S8	Ii 2	-5.6	142.3	8.7	10	s
17-S-15	Gj 3	-2.1	231.5	3.5	5	s	17-S8	Ij 1	-11.9	131.5	15.9	9	s
17-S-15	Gj 4	-0.8	228.2	1.4	6	s	17-S8	Ij 2	-10.7	130.3	14.7	5	s
17-S-15	Gj 5	-0.8	228.2	1.4	5	s	17-S8	Ij 3	-10.0	131.5	14.0	5	s
17-S-15	Gj 6	-1.0	227.0	1.7	5	s	17-S8	Ik 1	-5.3	155.3	8.3	6	s
17-S-15	Gj 7	-0.9	227.0	1.5	4	s	17-S8	Ik 2	-7.9	177.3	11.5	-	s
17-S-15	Gk 1	-4.5	239.1	7.2	-	s	17-S8	Ik 3	-3.1	187.3	5.2	-	s
17-S-15	Gk 2	-4.2	237.5	6.8	-	s	17-S8	Ik 4	-2.7	172.2	4.4	-	s
17-S-15	Gl 1	-6.1	211.3	9.3	-	s	17-S8	Ik 5	-3.1	163.9	5.2	-	s

Notes: dashes = no values recorded, A# = assemblage, T_m^{ice} = ice melting temperature, $T_h^{L+V \rightarrow L}$ = temperature of homogenization, S wt% NaCl eq corresponds to salinity wt% values, s = secondary, u = uknown

5.0 Discussion

5.1 Comparison of the Goldy and Irene showings

The studied mineral showings show some similarities in terms of their mineralogy, fluid inclusion microthermometry, and mineral thermometry. The dissimilarities may be the result of differences in fluid pressure and temperature, fluid source, distance from fluid source, or heat source.

The gangue and precious/base metal mineral assemblage at the Goldy showing is comprised of (i) carbonate hosted (VG1) pyrite, arsenopyrite, sphalerite, and +/- tetrahedrite-tennantite; (ii) quartz hosted (VG2) pyrite, chalcopyrite, galena, +/- rutile and boulangerite; (iii) late stage arsenopyrite-rich "blue quartz" breccia (VG3), and (iv) and later barren chalcedony veins (VG4). At the Irene property, veins are comprised of (i) quartz-carbonate hosted (V1) pyrite, arsenopyrite, galena, stibnite, electrum, and a variety of Sb-sulfides (sorbyite, kobellite, vikingite, and hakite); (ii) Fe,Mg-carbonate hosted (V2) pyrite, chalcopyrite, galena, rutile, and boulangerite, and; (iii) late stage (V3) arsenopyrite-rich "blue quartz" breccia. Therefore, the mineralogy and sequence of veins are very similar, but with a Cu-Zn-Pb-As association at Goldy and Pb-Sb-As mineralogical association at Irene.

These assemblages, in particular the chalcedonic quartz and quartz-carbonate veining hosting sulfides such as stibnite, pyrite, and arsenopyrite, are characteristic of shallow (0-300m depth) low sulfidation systems (Hedenquist, 2000). The gangue mineralogy observed in quartz-carbonate veins (VG1 and V1-types) with mineralogy barite, galena, sulfosalts, and tetrahedrite-tennantite are characteristic of deeper (300-

40

800m depth) low sulfidation styles (Hedenquist, 2000). Neither of these properties fit uniquely into either category, possibly indicating that both showings underwent multiple phases of mineralization at varying confining depths, or that local fluid interactions with host rocks influenced the mineralization composition.

The fluids from Goldy, ranging between 0-6 wt% NaCl eq, with $T_h^{L+V \rightarrow L}$ temperatures of between 200-250 °C are consistent with low sulfidation deposits, whereas the fluids from Irene, ranging from 5-15 wt% NaCl eq, and with $T_h^{L+V \rightarrow L}$ of 140-230 °C are at the upper boundary (but still within) the range for deep low sulfidation deposit type (Hedenquist, 2000).

Overall, with a combination of both shallow and deep low sulfidation characteristics, these properties can be considered as hosting intermediate to low sulfidation mineralization which is also supported by the fluid inclusion classification parameters summarized by Bodnar et al. (2014) (Fig. 13).

A summary of the geological settings and other definitive characteristics, as well as several global examples of typical epithermal Au deposit subtypes, is summarized by Taylor (2007). From those examples, a low-sulfidation system is hosted in a sedimentary and/or mixed host rock setting and that shares an ore mineralogy similar to the Goldy and Irene showings (electrum, Sb-sulphides, with quartz and calcite gangue). The fluid compositions at Goldy and Irene supports this, with a less than ≤15 wt % NaCl eq and homogenization ($T_h^{L+V \rightarrow L}$) ranging from 200-240 °C.

To the extent that similar mineral assemblages result from a common mineralizing fluid, the Goldy and Irene showings both have pyrite, arsenopyrite (with an overlapping

As composition) (Fig. 10), barite, rutile, sphalerite, galena, Sb-sulphides, and precious metal mineralization (though different carriers of Au). A common ore mineralogy suggests similar mineralizing fluids in terms of accessory and ore metal content.

The intersections between the fluid inclusions P-T isochores and the thermometric values from As at% compositions of arsenopyrite (Fig. 14) indicate an erroneous mineralizing depth of ~3-12 kilometers. This depth is inconsistent with an epithermal mineralization style, and considering the relatively low metamorphic grade (greenschist to lower amphibolite facies; Payne et al., 1987) for the host assemblages. This suggests that the hydrothermal fluids were trapped in quartz at temperatures lower than arsenopyrite growth, rendering the intersection invalid. It appears that conditions of early arsenopyrite crystallization within the T window 400-420°C preceded entrapment fluids lower temperatures as quartz was crystallizing. Fluid inclusions are not coeval with arsenopyrite, and two hydrothermal events are suggested with gold associated with both the high T (asp) 400-420°C and low T events (quartz-Sb mineralization) 150-250°C.

This leads to speculation on why the salinities between both showings vary. The intersection observed in the P-T diagram (Fig. 14) suggest that the hydrothermal fluids at the Irene property were ~50 to 100°C cooler than those of the Goldy property under an isobaric regime, or a pressure difference of ~1-1.5 kbar under an isothermal regime. This pressure difference would require the Irene property to be subjected to approximately 3 km of cover rock which has since been eroded. This speculation is not likely given the proximity of the two showings (10 km) and the erroneous P-T intersections, suggesting the variation in salinities are due to differing involvements of meteoric vs. magmatic-hydrothermal fluids.

5.2 Other mineralogical constraints on vein formation

At the Irene showing Sb-sulfides and sulfosalts are observed in higher abundances relative to Goldy. Correlation data (Fig. 4) suggest a significant correlation (r = 0.8, n = 700) between Au and Sb which is supported by petrographic observations (Fig.8e) where gold is occurring as inclusions in Sb-sulfides. This suggests that the hydrothermal fluids mineralizing Au- and Sb-minerals are sulfide buffered (and so bisulfide is the ligand for both Au and Sb) showing a progressive decrease in S activity with time (Williams-Jones and Normand, 1997). Hydrothermal fluids that are saturated in hydroxothioantimonite $[Sb_2S_2(OH)^0_2]$ precipitate stibnite and Sb-bearing minerals in response to conductive cooling which consumes H_2S initiating Au precipitation (Au carried in a $Au(HS)^-_2$ complex; (Krupp, 1988; Rottier et al., 2018). The solubility of Sb is controlled strongly by temperature, and so this suggests that stibnite or other Sb-bearing minerals are present, the fluid had to start out at high temperatures (>350°C) and then cool to precipitate Sb minerals (Williams-Jones and Normand, 1997). The coprecipitation of stibnite and gold may also indicate that the pH of the system decreased with time (Williams-Jones and Normand, 1997). Theoretical and experimental data suggest that for the Sb and As end-members of tetrahedrite-tennantite, the Sb-end member (tetrahedrite) is more stable at lower temperatures and the As-end member (tennantite) is more stable at higher temperatures (Seal et al., 1990). The As-rich Goldy mineralization may be a higher temperature expression of the system. Additionally, at higher temperatures arsenic complexes may also contribute to gold solubility, possibly relevant to the Goldy showing

(McCuaig and Kerrich, 1998). The hih T vs. low T differences in As vs. Sb tenor are consistent with the fluid inclusion $T_h^{L+V \to L}$ data.

5.3 Comparison of the showings to other epithermal deposits in the Cordillera

The subduction and collisional geologic history of the Canadian Cordillera is a prime setting for many porphyry-epithermal systems. Fluid inclusion data and mineralogy of Goldy and Irene are comparable to major low- to intermediate-sulfidation systems in the Cordillera. Fluid inclusion data and mineralogy from these showings are best compared to the epithermal Au-Ag deposits at Mount Skukum (McDonald, 1987); Sulphurets (Margolis, 1993) Black Dome (Vivian et al., 1987); Mallery Lake (Turner et al., 2001) and Dusty Mac although the studies showings have a slightly lower in T than the Dusty Mac deposit in BC (230-250 °C) (Zhang et al., 1989)

6.0 Conclusion and implications for exploration

The mineralogy in both showings show some major similarities but with differences related to fluid evolution. Goldy is richer in arsenopyrite which is likely to host gold in a dissolved state (Fig. 4), whereas Irene is rich in Sb-sulfides and sulfosalts which are associated with gold as electrum in pyrite-hosted inclusions (Fig. 8). The fluid inclusion analyses conclude that Irene is a slightly deeper and cooler ($T_h^{L+V \to L}$ = 130.3° to 232.5°C; $T_h^{L+V \to L}$ = 178.9° to 247.7°C) system involving more saline fluids (2.9 to 22.7 wt% NaCl eq; 0.7 to 16.4 wt% NaCl eq) compared to the Goldy system. The Goldy showing may

have been closer a heat source and had greater involvement with meteoric water which may have triggered Au precipitation (Nesbitt et al., 1986).

The likelihood that Goldy and Irene constitute part of a single hydrothermal system with a common heat source is high. However, the uncertainty remains whether the two showings are the result of varying pressure and temperature regimes or if there is a temporal or telescoping effect in the system. Two different mineralizing events are proposed: a high T event involving As-Au association, and a lower T event, more consistent with epithermal conditions involving an Sb-Au association that is more pronounced at the Irene showing.

When considering developing these properties, the processing of ore materials and their associated minerals has to be taken in to consideration. In the Goldy property the coupling with arsenopyrite might prove to be an issue as processing arsenic-rich materials has environmental concerns and associated additional costs (Robins and Jayaweera, 1992).

References

Bineli, B. T., Lentz, D. R., & McFarlane, C. (2016). The Nucleus Deposit: Superposed Au-Ag-Bi-Cu Mineralization Systems at Freegold Mountain, Yukon, Canada. *Resourse Geology*, 419-454.

Bodnar, R., & Vityk, M. (1994). *Interpretation of Microthermometric Data for H2O-NaCl Fluid Inclusions.*

Bodnar, R., Lecumberri-Sanchez, P., Moncada, D., & Steele-MacInnis, M. (2014). Fluid Inclusions in Hydrothermal. In *Treatise on Geochemistry* (2nd ed., Vol. 13, pp. 119-142). Oxford: Elsevier.

Bodnar, R., Lecumberri-Sanchez, P., Moncada, D., & Steele-MacInnis, M. (2014). Fluid Inclusions in Hydrothermal Ore Deposits. In H. Holland, & K. Turekian, *Treatise on Geochemistry* (Vol. 13, pp. 119-142). Oxford: Elsevier. doi:10.1016/B978-0-08-095975-7.01105-0

Carlson, G. G. (1987). Geology of Mount Nansen and Stoddart Creek map areas Dawson Range, Central Yukon. *Exploration and Geological Services Division, Yukon Region, Indian and Northern Affairs Canada*, 181.

Colpron, M. N., Nelson, J. L., & Murphy, D. C. (2006). A tectonostratigraphic framework for the Pericratonic terranes of the northern Canadian Cordillera. *Geological Association of Canada*, 1-23.

Friend, M., Allan, M., Israel, S., Colpron, M., Crowly, J., & Hart, C. (2018). *Preliminary results from field investigations in the Freegold district, Dawson Range, Yukon.* MDRU.

Goldstein, R. (2003). Petrographic analysis of fluid inclusions. *Mineralogical Association of Canada, Short Course Series, 32*, 9-54.

Hedenquist, J. W. (2000). Exploration for epithermal gold deposits. *SEG Reviews, 13*, 243-277.

Kretschmar, U., & Scott, S. D. (1976). Phase relationsinvolving arsenopyrite in the system Fe-As-S and their application. *Can. Mineral*(14), 364-386.

Krupp, R. (1988). Solubility of stibnite in hydrogen sulfide solutions, speciation, and equilibrium constants, from 25 to 350°C. *Geochimica et Cosmochimica Acta, 52*(12), 3005-3015. doi:10.1016/0016

LeBarge, W. (1995). Sedimentology of Placer Gravels Near Mount Nansen, Central Yukon Territory. *Indian and Northern Affairs Canada, Yukon*(4), 155.

Margolis, J. (1993). *Geology and Intrusion-Related Copper-Gold Mineralization, Sulphurets, British Columbia.* University of Oregon, Eugene, Oregon.

Matas, S. G., Allan, M. M., Hart, C. J., & Mortensen, J. K. (2014). *Structural and tectonic control on mineralization by magnetite-destructive faultsin western Yukon and eastern Alaska.* Mineral Deposit Research Unit, University of British Columbia, 2020 - 2207 Main Mall, Vancouver, BC V6T 1Z4, Canada. The Geological Society of America (GSA).

McCuaig, T., & Kerrich, R. (1998). P-T-t-deformation-fluid characteristics of lode gold deposits:. *Ore Geology Reviews, 12*, 381-453.

McDonald, B. (1987). *Geology and Genesis of the Mount Skukum Tertiary Epithermal Gold-Silver Vein Deposit, southwestern Yukon.* University of British Columbia.

Moncada, D., Mutchler, S., Nieto, A., Reynolds, T., Rimstidt, J., & Bodnar, R. (2012). Mineral textures and fluid inclusion petrography of the epithermal Ag-Au deposits at Guanajuato, Mexico: Application to exploration. *Jornal of Geochemical Exploration*(114), 427-435.

Monger, J., Price, R., & Nokleberg, W. (2004). *Encyclopedia of Geology* (Vol. 4). (R. C. Selley, L. R. Cocks, & I. R. Plimer, Eds.) Elsevier, Oxfird.

Mortensen, J. (1992, August). Pre-Mid-Mesozoic tectonic evolution of the Yukon-Tanana Terrane, Yukon and Alaska. *Tectonics, 11*(4), 836-853. doi:https://doi.org/10.1029/91TC01169

Nesbitt, B., Murowchick, J., & Muehlenbachs, K. (1986). Dual origins of lode gold deposits in the Canadian Cordillera. *Geology, 14*(6), 506-509. doi:10.1130/0091

Northern Freegold Resources Ltd. (2007). *2007 Drilling assessment Report.*

Payne, J., Gonzalez, R. A., Akhurst, K., & Sisson, W. G. (1987). Geology of Colorado Creek, Selwyn River, and Prospector Mountain map areas, western Dawson Range, west-central Yukon. *Exploration and Geological Services Division, Idian and Northern Affairs Canada, Yukon*, 141.

Price, R. A. (1986). The southeastern Canadian Cordillera: Thrust faulting, tectonic wedging, and delamination of the lithosphere. *Journal of Structural Geology*, 239-254.

Robins, R., & Jayaweera, L. (1992). Arsenic in Gold Processing. *Mineral Processing and Extractive Metallurgy Review, 9*(1-4), 255-271. doi:10.1080/08827509208952710

Rottier, B., Kouzmanov, K., Casanova, V., Wälle, M., & Fontboté, L. (2018). Cyclic Dilution of Magmatic Metal-Rich Hypersaline Fluids by Magmatic Low-Salinity Fluid: A Major Process Generating the Giant Epithermal Polymetallic Deposit of Cerro de Pasco, Peru. *Economic Geology, 113*(4), 825-856. Retrieved from https://doi.org/10.5382/econgeo.2018.4573

Scott, S. (1983, December). Chemical behaviour of sphalerite and arsenopyrite. *Mineralogical Magazine, 47*, 427-435.

Seal, R., Essene, E., & Kelly, C. (1990). Tetrahedrite and tennantite: evaluation of thermodynamic data and phase equilibra. *Canadian Mineralogist, 28*, 725-738.

Smuck, K. A. (1999). *Metallogeny of Epithermal Gold and Base Metal Veins of the Southern Dawson Range, Yukon.* Montreal, Quebec, Canada: Department of Earth and Planetary Sciences McGIll University.

Taylor, B. E. (2007). Epithermal Gold Deposits. *Geological Association of Canada*(5), 113-139.

Triumph Gold Corp. (2019, January). *Triumph Gold Announces Results from Inaugural Drilling of the Irene Gold Vein, Defining Mineralization over 450 Metres with Gold Grades up to 20.7 grams per tonne.* (T. Baressi, Ed.) Retrieved from Triumph Gold Corp: www.triumphgoldcorp.com

Turner, W., Richards, J., Nesbitt, B., Muehlenbachs, K., & Biczok, J. (2001). Proterozoic low-sulfidation epithermal Au-Ag mineralization in the Mallery Lake area, Nunavut, Canada. *Mineralium Deposita, 36*, 442-457.

Vivian, G., Morton, R., Changkakoti, A., & Gray, J. (1987). Blackdome Eocene epithermal Ag− Au deposit, British Columbia, Canada—nature of ore fluids. *Applied Earth Science, 96*, B9-B14.

Williams-Jones, A., & Normand, C. (1997). Controls of Mineral Parageneses in the System Fe-Sb-S-O. *Economic Geology, 92*, 308-324.

Zhang, X., Nesbitt, B. E., & Muehlenbachs, K. (1989). Gold mineralization in the Okanagan Valley, southern British Columbia; fluid inclusion and stable isotope studies. *Economic Geology*(84), 410-424. doi: doi: https://doi.org/10.2113/gsecongeo.84.2.410

Appendix 1: Petrographic Descriptions

Irene

MMFGR180

This sample is taken from a granitoid rock with significant silicification and mineralization. The host is composed of varied in size equigranular quartz and sericite alteration of host mineral hosting euhedral rhombic arsenopyrite. There is a V1-type vein that has equigranular hydrothermal quartz in textural equilibrium with calcite. This vein hosts stibnite mineralization with cuspate margins.

qtz: 60%, 20% stib, carb: 5%, asp: 2%, clays: 13%

MMFGR181

This sample is from a high grade off shoot, potentially hosted in a granitoid rock. Significant alteration present with initial V2-type cockade texture carbonate veining that have later been infilled and brecciated by V3-type fine grain quartz. The V3-type vein is hosting minor cuspate stibnite. The carbonitization is pervasive with semi pervasive silicification.

qtz: 50, carb: 50, opaques: 1%

IR17-S1

This sample is from a slightly altered biotite granodiorite. The biotite and minor hornblend have been sericitized and host anhedral pyrite and mymekitic tecture galena. Semi-pervasive V2-type veining.

carb: 50%, qtz: 20%, kaolinite: 10%, py: 5%

IR17-S2

This sample is from a significantly silicified rock. Initial semi pervasive V2-type veining of dolomite is present that is hosting cuspate stibnite with trace boulangerite with a surrounding void, indicating decrease in volume. Subsequent V3-type quartz flooding is present which is also hosting minor stibnite.

IR17-S3A

This sample is from a quartz-carbonate breccia from a highly altered protolith. There appears to be several generations of V2-type and V3-type veining occurring. The carbonate veining is equigranular with a comb orientation with little mineralization. The V3-type veining is massive to comb texture with mineralization of galena, sphalerite, bornite, chalcopyrite, and minor tetrahedrite. Semi-pervasive late hematite V4-type veining.

carb: 20%, qtz: 60%, kaolinite: 10%, py: 5%, gal/sph: 5%tite veining.

IR17-S4

This sample is taken from an intruding quartz-feldspar-porphyry dyke that is prevalent throughout the Freegold Mountain property. It is a fine grain groundmass of massive quartz with isolated calcite. The feldspars have been altered and sericitized.

IR17-S5

This sample is highly silicified and brecciated. There is pervasive V3-type veining that has brecciated inferred V2-type veins given the isolated carbonate fragments. Euhedral arsenopyrite is conventrated in the V3 groundmass with a fragment of anhedral pyrite with sphalerite replacement texture.

carb: 40%, qtz: 40%, sulfides: 20%

IR17-S6

Altered biotite hornblend granodiorite. There is pervasive silicification of V3-type fine grain quartz that contains fragments of V2-type veins. Late whispy calcite veinlets present with no mineralization. In the V3 groundmass there is minor arsenopyrite and pyrite.

qtz: 45% carb: 45%, sulfides: 10%

IR17-S8

Relatively unaltered biotite-hornblend granodiorite. Equigranular texture of plagioclase-feldspar-quartz-biotite with semi-pervasive V2-type veining with mineralized chalcopyrite and sphalerite.

 qtz: 30, fsp: 50, mica: 15, sulfides: 5%

IR17-S9

Granodiorite host. This sample contains a mineralized V1-type vein with mineralized amorphous electrum (85% Au, 15% Ag) in special and textural association with lead-antimony mineralization.

Goldy

GLD17-S1: 34m

This sample is part of the Yukon Tanana metasedimentary unit. The wall rock is significantly altered to sericite minerals. There is pervasive veining throughout with cross-cutting relationships between the VG1-type vein with low arsenopyrite and sphalerite mineralization – arsenopyrite appears to be altering to sphalerite. What appears to be coeval jigsaw carbonate VG2-type veining being cross-cut by massive quartz VG3-type veining, and a last generation of VG4-type quartz veining with plumose margins and a massive fill, representing chalcedonic quartz. This sample is relatively low mineralized.

qtz: 70%, ser: 30%, asp-sph: >1%

GLD17-S2: 35.6m

This sample is part of the Yukon Tanana metasedimentary unit that is heavily altered to sericite. There has been semi-pervasive silicification with VG4-type veining.

GLD17-S3: 39.52m

Heavily altered Yukon Tanana host rock with pervasive chalcedonic VG4-type veining. Sericitized vein margin with host rock. No mineralization.

GLD17-S4: 44.11m

Altered syenite host rock with felspars altering to clay. VG2 type quartz vein with sphalerite mineralization.

GLD17-S5: 54.7m

This sample represents the syenite unit. Alteration of hornblends and plagioclase to sericite but retain morphology. Chalcopyrite mineralization in VG2-type vein and is constrained to the margins of the vein – wall rock interface with euhedral polygonal shape.

GLD17-S6: 64.75m

Altered syenite host rock with sericitized felspars and hornblende. Trace pyrite mineralization in host rock which is mostly sericitized/altered to clay minerals.

GLD17-S7: 69.6m

Heavily altered syenite. Altered hornblende and plagioclase to sericite minerals. Pervasive hexagonal pyrite replacing and formed in altered minerals appears before VG3 and may be due to VG1 or 2 fluids. Crosscutting relationship between initial VG2-type vein with little mineralization and fine grain massive quartz VG3-type veining. Fracture filling tennenite-tetreahedire mineralization in pyrite associated with carbonate (dolomite) VG1-type veining.

GLD17-S8: 80.8m

Yukon Tanana metasedimentary host. Heavily altered host minerals to sericite then silicification. Pyrite and minor sphalerite is constrained to altered host minerals (biotite?).

qtz: 55% ser: 40% py: 5%

GLD17-S10: 101.8m

This sample is from a heavily altered and silicified hornblendite unit. The altered host minerals are significantly altered and hosting euhedral arsenopyrite mineralization that is being replaced by galena and sphalerite.

GLD17-S11: 104.6m

Faint outlines of felspars altered to clays indicating a syenite host. Pervasive quartz VG3-type veining hosting angular arsenopyrite

GLD17-S12: 107.3m

Heavily altered syenite. Host minerals have been altered to sericite and host arsenopyrite mineralization that is in textural equilibrium with pyrite, which has anhedral blebby texture, and +/- rutile. A cross-cutting VG4-type vein with no mineralization.

GLD17-S13: 108.65m

Altered syenite. Pyrite and arsenopyrite mineralization in VG2-type vein with same textures found in altered host minerals with sphalerite replacing sphene (davanite) crystal in special relationship with arsenopyrite. VG1-type vein with sphalerite mineralization.

qtz: 60% ser: 30% sulfides: 8% carb: 2%

GLD17-S14: 111.24m

Heavily altered host with pervasive fine grain and euhedral quartz veining throughout. VG1-type veining with sphalerite mineralization with sericitized wall rock margins. Beyond the sphalerite mineralization the sample is barren

GLD17-S15: 114.3m

Altered host rock with pervasive quartz veining. Cross-cutting relationship with VG1-type carbonate veining and VG3-type quartz breccia. VG3-type veining hosting sphalerite mineralization that is replacing arsenopyrite. Carbonate mineralization is euhedral with no mineralization. Altered wall rock is being replaced by pyrite and arsenopyrite mineralization. This sample was used to fluid inclusions analysis.

qtz: 60% ser: 30% sulfides: 8% carb: 2%

GLD17-S16: 119.1m

Yukon Tanana host rock with heavy alteration. Host minerals have altered and sericitized with possible carbonate replacement mineralization from VG1-type fluids. Arsenopyrite, pyrite, sphalerite, and minor chalcopyrite mineralization seen in fracture filling and mineral replacement.

qtz: 40% ser: 30% carb: 25% sulfides: 5%

GLD17-S-S1:

Quartz breccia with chalcedonic quartz VG4-type cross-cutting vein. The fine grain quartz VG3-type vein hosting arsenopyrite mineralization in addidtion to wall rock fragments. The VG4-type veining shows coxcomb textures and void of mineralization.

qtz: 95% sulfides: 5%

GLD17-S-S2:

Predominantly quartz from VG3-type flooding. The fine-grained quartz is hosting altered wall rock fragments containing mostly arsenopyrite with minor sphalerite mineralization.

qtz: 99% sulfides: ~1%

GLD17-S-S4

Heavily altered host rock, possibly Yukon Tanana. This section displays significant alteration of host minerals to clays and pervasive silicification. Minor pyrite mineralization is present in wall rock minerals however, beyond that is void of significant mineralization.

GLD17-S-S5

Yukon Tanana host rock with VG4-type veining void of mineralization cross-cutting VG1-type veining mm- to >-mm in size without significant mineralization. Pyrite growth in the wall-rock is observed showing blebby texture. This sample was used for fluid inclusion analysis.

Appendix 2a: Assay results, Goldy

Hole ID	Depth from (m)	Depth to (m)	Au (ppm)	Ag (ppm)	Bi (ppm)	Cu (ppm)	Pb (ppm)	Sb (ppm)	Zn (ppm)	As (ppm)
07GY-16	4.2	5.9	0.01	0.4	-5	5	386	20	1201	2415
07GY-16	5.9	8.7	0.01	-0.2	-5	3	16	-5	45	195
07GY-16	8.7	9.1	0.04	0.7	-5	5	350	20	318	1230
07GY-16	9.1	11.3	0.01	1	-5	30	86	20	177	35
07GY-16	11.3	11.45	0.01	1.3	-5	33	92	25	424	105
07GY-16	11.45	12.6	0.015	0.3	-5	2	158	10	127	55
07GY-16	12.6	13.8	0.005	0.4	5	5	144	20	221	110
07GY-16	13.8	14.3	0.505	0.7	-5	4	324	15	494	945
07GY-16	14.3	16.7	0.12	0.5	-5	2	144	20	440	750
07GY-16	16.7	18	0.78	0.4	-5	7	114	10	253	2165
07GY-16	18	18.65	0.12	1.4	25	12	410	55	1193	3530
07GY-16	18.65	19.6	2.17	0.2	-5	5	60	5	118	2330
07GY-16	19.6	21.3	0.105	0.3	-5	6	58	10	181	790
07GY-16	21.3	22.85	0.015	7.2	-5	40	192	20	155	165
07GY-16	22.85	23.4	0.005	0.7	-5	111	214	30	435	160
07GY-16	23.4	25.2	0.025	0.5	-5	3	102	5	274	175
07GY-16	25.2	26.6	0.015	0.6	-5	5	252	20	277	185
07GY-16	26.6	28.05	0.035	1	-5	10	244	20	162	255
07GY-16	28.05	28.8	0.015	0.6	-5	19	78	15	263	325
07GY-16	28.8	29.6	0.02	1	-5	32	168	55	548	390
07GY-16	29.6	30.6	0.005	0.4	-5	48	48	20	262	145
07GY-16	30.6	32.8	0.015	-0.2	-5	20	16	-5	64	40
07GY-16	32.8	34	0.025	0.5	-5	44	78	45	180	210
07GY-16	34	35.1	0.01	0.3	-5	70	14	10	60	80
07GY-16	35.1	36.6	0.01	-0.2	-5	15	18	5	68	75
07GY-16	36.6	38.1	0.005	0.3	-5	9	24	-5	80	40
07GY-16	38.1	38.6	0.015	0.2	-5	7	12	-5	24	45
07GY-16	38.6	40.35	0.01	0.2	-5	30	18	-5	73	35
07GY-16	40.35	40.7	0.01	0.5	-5	89	34	10	180	30
07GY-16	40.7	42.1	0.02	-0.2	-5	25	24	20	57	105
07GY-16	42.1	43.7	-0.005	-0.2	-5	11	18	10	31	30
07GY-16	43.7	45.3	0.015	-0.2	-5	6	18	15	36	60
07GY-16	45.3	46.95	0.01	-0.2	-5	30	16	-5	35	25
07GY-16	46.95	48.6	0.01	-0.2	-5	49	20	10	69	20
07GY-16	48.6	50.3	0.02	-0.2	-5	31	16	-5	29	55
07GY-16	50.3	51.9	0.045	-0.2	5	7	20	10	54	330
07GY-16	51.9	53.5	0.025	-0.2	-5	6	24	25	76	135
07GY-16	53.5	55	0.02	-0.2	-5	8	24	25	63	360
07GY-16	55	56.2	0.04	-0.2	-5	9	22	20	59	520
07GY-16	56.2	57.6	0.11	0.2	-5	7	22	20	61	495
07GY-16	57.6	59.5	0.01	-0.2	-5	6	12	15	40	125
07GY-16	59.5	60.95	0.01	-0.2	-5	6	14	-5	51	40
07GY-16	60.95	62.3	0.035	-0.2	-5	5	16	5	61	30
07GY-16	62.3	63.7	0.05	-0.2	-5	5	20	15	73	125
07GY-16	63.7	65.15	0.025	-0.2	-5	5	26	20	76	95
07GY-16	65.15	66.5	0.01	0.2	-5	4	18	10	81	55
07GY-16	66.5	67.05	0.04	0.2	5	4	12	10	37	105

Hole ID	Depth from (m)	Depth to (m)	Au (ppm)	Ag (ppm)	Bi (ppm)	Cu (ppm)	Pb (ppm)	Sb (ppm)	Zn (ppm)	As (ppm)
07GY-16	67.05	68.6	0.025	-0.2	10	3	14	10	36	70
07GY-16	68.6	70.1	0.015	0.3	-5	17	14	10	35	55
07GY-16	70.1	71.2	0.015	0.5	-5	17	12	10	42	65
07GY-16	71.2	72.3	0.025	0.8	-5	5	76	-5	342	700
07GY-16	72.3	74.1	0.215	0.3	20	13	94	25	155	70
07GY-16	74.1	75.85	0.015	0.4	20	14	52	65	127	80
07GY-16	75.85	77	0.02	0.3	-5	5	22	5	161	155
07GY-16	77	77.7	0.075	0.3	-5	10	26	20	126	280
07GY-16	77.7	79.3	0.235	0.8	-5	8	38	15	233	1180
07GY-16	79.3	80.4	0.01	0.6	-5	20	36	25	148	270
07GY-16	80.4	81.9	0.17	1.8	-5	16	28	20	82	815
07GY-16	81.9	83	0.05	0.5	-5	7	34	15	186	810
07GY-16	83	84	0.06	0.3	-5	7	28	25	176	735
07GY-16	84	85	0.005	0.4	10	16	34	35	174	85
07GY-16	85	86	0.075	0.2	-5	15	30	-5	78	455
07GY-16	86	86.9	0.005	0.3	-5	6	22	10	107	90
07GY-16	86.9	88.1	0.01	0.3	-5	8	22	20	69	120
07GY-16	88.1	89.5	0.005	0.3	-5	6	32	10	137	245
07GY-16	89.5	91	0.005	0.5	-5	3	20	20	54	85
07GY-16	91	92.5	-0.005	0.3	-5	2	24	10	133	150
07GY-16	92.5	93.7	-0.005	-0.2	-5	2	34	15	126	45
07GY-16	93.7	93.9	0.005	1	-5	16	28	20	125	195
07GY-16	93.9	95	-0.005	-0.2	-5	16	28	20	72	105
07GY-16	95	95.7	0.035	-0.2	-5	14	50	15	234	735
07GY-16	95.7	96.8	-0.005	0.3	-5	28	16	15	31	40
07GY-16	96.8	97.9	-0.005	0.2	-5	9	128	-5	364	455
07GY-16	97.9	98.6	-0.005	0.8	-5	49	368	35	974	1270
07GY-16	98.6	100	-0.005	0.8	5	27	158	25	937	225
07GY-16	100	100.85	0.005	0.3	-5	6	436	30	2285	1090
07GY-16	100.85	102	0.97	2	-5	20	720	30	2921	5720
07GY-16	102	103	0.21	0.4	-5	7	156	15	1066	2065
07GY-16	103	104.55	9.63	0.2	-5	7	114	15	609	5520
07GY-16	104.55	105.7	1.83	-0.2	-5	3	50	5	486	4390
07GY-16	105.7	106.15	13.7	0.8	5	20	208	65	1240	10000
07GY-16	106.15	106.8	6.92	0.6	-5	18	236	35	186	5145
07GY-16	106.8	108	38	1.4	15	27	760	80	1696	10000
07GY-16	108	109.3	14.5	1	20	14	588	175	2894	10000
07GY-16	109.3	110.2	24	0.6	15	20	716	105	3402	10000
07GY-16	110.2	111.2	4.13	1	10	28	294	70	1126	10000
07GY-16	111.2	112.3	23.5	1.3	15	15	438	70	2228	10000
07GY-16	112.3	113.3	0.82	1.4	10	10	380	30	922	1880
07GY-16	113.3	114.3	2.66	0.8	20	7	230	30	565	2975
07GY-16	114.3	116.3	0.03	0.2	10	14	50	20	70	80
07GY-16	116.3	118.2	0.03	0.4	10	12	48	45	78	155
07GY-16	118.2	119.2	2.95	6.5	-5	21	1896	345	2833	10000
07GY-16	119.2	119.9	1.91	1.5	10	9	518	55	572	4515
07GY-16	119.9	120.5	0.15	4.2	-5	18	1114	170	1693	5235
07GY-16	120.5	121	0.03	0.4	10	14	58	40	262	90
07GY-16	121	122.5	0.09	0.4	-5	8	142	20	199	500
07GY-16	122.5	124	0.025	0.2	-5	6	34	25	111	75
07GY-16	124	124.4	0.02	-0.2	5	6	30	20	98	95
07GY-16	124.4	124.75	0.025	-0.2	-5	10	38	35	141	110

Hole ID	Depth from (m)	Depth to (m)	Au (ppm)	Ag (ppm)	Bi (ppm)	Cu (ppm)	Pb (ppm)	Sb (ppm)	Zn (ppm)	As (ppm)
07GY-16	124.75	125.5	0.01	0.2	-5	5	30	10	127	80
07GY-16	125.5	126.9	0.01	-0.2	5	12	78	50	279	195
07GY-16	126.9	128.6	0.03	0.5	15	18	58	35	304	170
07GY-16	128.6	129.2	0.03	0.2	10	4	134	25	387	325
07GY-16	129.2	129.65	0.015	0.4	5	16	54	50	114	50
07GY-16	129.65	130.8	0.015	0.5	-5	19	68	10	217	75
07GY-16	130.8	132	0.035	0.8	-5	6	190	15	394	280
07GY-16	132	133	1.48	3	10	10	1290	55	1158	2890
07GY-16	133	134	1.48	1.5	-5	4	500	30	1139	4615
07GY-16	134	134.7	0.09	0.8	-5	3	496	-5	1340	2865
07GY-16	134.7	135.1	0.015	0.3	-5	3	96	20	164	750
07GY-16	135.1	136.8	0.015	0.2	-5	1	106	15	229	60
07GY-16	136.8	137.9	0.125	1	-5	5	734	45	1875	1450
07GY-16	137.9	139	0.11	2.1	-5	11	808	45	2217	2985
07GY-16	139	140.5	0.135	0.9	10	4	406	30	1827	1470
07GY-16	140.5	141.7	5.1	1.6	-5	8	1220	45	4171	6195
07GY-16	141.7	142.9	1.78	1.2	-5	5	440	20	980	4670
07GY-16	142.9	143.8	8.1	2.4	-5	6	726	30	1763	7605
07GY-16	143.8	144.75	0.575	1.8	-5	6	572	25	1193	3725
07GY-16	144.75	146.5	0.26	1.3	-5	5	448	10	1458	4015
07GY-16	146.5	147.6	0.04	0.7	-5	8	196	20	732	1380
07GY-16	147.6	148.65	0.015	0.6	-5	5	86	20	312	1080
07GY-16	148.65	149.45	0.225	0.8	-5	5	186	25	658	3580
07GY-16	149.45	150.6	10.1	5.6	-5	21	858	105	1774	6620
07GY-16	150.6	151.8	0.21	1.4	10	7	196	45	759	915
07GY-16	151.8	153	0.91	-0.2	15	8	160	30	894	6490
07GY-16	153	154.4	0.025	-0.2	15	4	40	30	147	95
07GY-16	154.4	155.45	0.38	-0.2	5	10	44	-5	86	615
07GY-16	155.45	157	0.055	-0.2	25	16	48	55	111	40
07GY-16	157	158.5	0.015	-0.2	-5	10	94	15	157	65
07GY-16	158.5	160	0.01	-0.2	-5	9	24	5	98	15
07GY-16	160	161.55	0.01	-0.2	5	7	32	15	97	10
07GY-16	161.55	163.1	0.005	-0.2	-5	9	14	-5	33	10
07GY-16	163.1	165.1	0.015	-0.2	-5	6	100	20	245	35
07GY-16	165.1	166.8	0.01	-0.2	-5	7	76	10	228	15
07GY-16	166.8	168	0.01	-0.2	5	10	60	-5	300	20
07GY-16	168	169.15	0.01	-0.2	5	8	18	10	99	-5
07GY-16	166.8	168	0.01	-0.2	5	10	60	-5	300	20
07GY-16	168	169.15	0.01	-0.2	5	8	18	10	99	-5

Appendix 2b: Assay results, Irene

Hole ID	Depth from (m)	Depth to (m)	Au (ppm)	Ag (ppm)	Bi (ppm)	Cu (ppm)	Pb (ppm)	Sb (ppm)	Zn (ppm)	As (ppm)
IR18-01	16.76	18.28		-2	-5	14.6	14	16	57	11
IR18-01	18.28	19.81	0.01	-2	-5	6.8	11	12	56	18
IR18-01	33.53	35.05	0.01	-2	-5	16.9	14	20	67	41
IR18-01	35.05	36.58	0.01	-2	-5	1.7	16	22	67	50
IR18-01	36.58	38.1	0.01	-2	-5	0.6	17	24	73	52
IR18-01	38.1	39.62	0.01	-2	-5	8.3	18	18	66	36
IR18-01	39.62	41.15	0.01	-2	-5	13.5	19	22	112	35
IR18-01	41.15	42.67	0.03	-2	-5	21.2	18	24	82	79
IR18-01	42.67	44.2	0.01	-2	-5	4.3	14	34	60	38
IR18-01	44.2	45.72	0.03	-2	-5	17.1	19	25	84	72
IR18-01	45.72	47.24	0.01	-2	-5	8.6	17	20	63	47
IR18-01	47.24	48.77	0.01	-2	-5	8	14	26	54	46
IR18-01	48.77	50.29	0.01	-2	-5	9	18	22	71	39
IR18-01	50.29	51.5	0.01	-2	-5	2.2	17	24	74	36
IR18-01	51.5	52.58	0.02	-2	-5	11.1	9	30	33	58
IR18-01	52.58	53.7	0.01	-2	-5	16.8	13	34	91	54
IR18-01	53.7	54.86	0.01	-2	-5	31.3	22	35	45	69
IR18-01	54.86	56.39	0.01	-2	-5	34.5	17	32	68	41
IR18-01	56.39	57.91	0.01	-2	-5	22.4	15	28	63	38
IR18-01	57.91	59.44	0.01	-2	-5	9.3	12	33	56	61
IR18-01	59.44	60.96	0.01	-2	-5	9.1	15	28	58	39
IR18-01	60.96	62.68	0.01	-2	-5	30.2	10	38	73	46
IR18-01	62.68	64.01	0.1	-2	-5	17.9	19	69	66	497
IR18-01	64.01	65	0.69	-2	-5	11	22	71	35	981
IR18-01	65	65.8	0.82	-2	-5	7.8	17	56	55	1810
IR18-01	65.8	66.5	2.51	-2	-5	5.6	17	97	64	4430
IR18-01	66.5	67.2	20.7	-2	-5	56	15	9310	64	6910
IR18-01	67.2	67.8	13.15	-2	-5	29	39	10000	81	6540
IR18-01	67.8	68.8	0.04	-2	-5	57.8	22	106	45	138
IR18-01	68.8	69.8	0.08	-2	-5	109	18	149	48	113
IR18-01	69.8	70.8	4.41	-2	-5	15.8	24	1970	52	5220
IR18-01	70.8	72	0.05	-2	-5	48.8	21	101	54	440
IR18-01	72	73.15	9.00E-03	-2	5	51.9	16	36	71	57
IR18-01	73.15	74.68	0.01	-2	-5	38.9	25	22	90	264
IR18-01	74.68	75.8	9.00E-03	-2	-5	34.5	23	46	61	106
IR18-01	75.8	76.84	7.00E-03	-2	-5	44.7	39	42	99	388
IR18-01	76.84	78	-5.00E-03	-2	-5	13.2	24	16	83	26
IR18-01	78	79.25	-5.00E-03	-2	-5	6.5	18	12	77	-3
IR18-01	79.25	80.77	5.00E-03	-2	-5	13.9	27	18	45	19
IR18-01	80.77	82.3	7.00E-03	-2	-5	21.1	32	12	57	21
IR18-01	82.3	83.82	0.01	-2	-5	226	15	69	74	78
IR18-01	83.82	85.34	0.01	-2	-5	135	16	13	101	31
IR18-01	85.34	86.87	0.01	-2	-5	22	32	21	53	52
IR18-01	86.87	88.39	9.00E-03	-2	-5	20	19	23	83	41
IR18-01	88.39	89.4	0.01	-2	-5	29	20	22	69	39
IR18-01	89.4	90.48	9.00E-03	-2	-5	12.3	22	24	70	51

Hole ID	Depth from (m)	Depth to (m)	Au (ppm)	Ag (ppm)	Bi (ppm)	Cu (ppm)	Pb (ppm)	Sb (ppm)	Zn (ppm)	As (ppm)
IR18-01	90.48	91.76	7.00E-03	-2	-5	10.8	28	13	98	48
IR18-01	91.76	92.96	8.00E-03	-2	-5	17.8	15	16	101	79
IR18-01	92.96	94.49	7.00E-03	-2	-5	6.6	26	19	47	49
IR18-01	96.01	97.54	6.00E-03	-2	-5	13.8	38	21	77	75
IR18-01	97.54	99.06	-5.00E-03	-2	-5	34.3	33	28	41	129
IR18-01	99.06	100.5	6.00E-03	-2	-5	37.6	36	15	28	113
IR18-01	100.5	102.1	-5.00E-03	-2	-5	28.8	34	12	27	77
IR18-01	102.1	103.6	0.02	-2	-5	77.4	18	16	49	80
IR18-01	103.6	105.1	0.96	14	36	468	339	113	73	10000
IR18-01	105.1	106.6	0.11	-2	-5	124	65	59	54	523
IR18-01	106.6	108.2	0.01	-2	-5	37.2	47	19	115	87
IR18-01	108.2	109.7	0.01	-2	-5	11	26	9	17	42
IR18-01	109.7	111.4	0.01	-2	-5	26.6	23	13	36	74
IR18-01	111.4	112.7	0.03	-2	-5	33.2	19	13	54	61
IR18-02	24.58	26.16	-5.00E-03	-2	-5	9.1	13	11	51	5
IR18-02	26.16	27.61	-5.00E-03	-2	-5	10.5	14	11	51	15
IR18-02	27.61	28.96	6.00E-03	-2	-5	14.5	11	12	57	12
IR18-02	48	49.5	0.01	-2	-5	52.2	11	34	61	59
IR18-02	49.5	51	0.01	-2	-5	19.2	10	24	348	53
IR18-02	51	52.2	0.06	-2	-5	31.2	17	40	63	64
IR18-02	66.6	68.1	0.02	-2	-5	2.7	11	16	43	29
IR18-02	68.1	69.2	0.01	-2	-5	2.5	8	14	47	27
IR18-02	69.2	70.7	0.01	-2	-5	12.9	9	14	44	33
IR18-02	76	77.42	0.01	-2	-5	4	21	13	36	47
IR18-02	77.42	78.5	0.01	-2	-5	102	12	21	36	522
IR18-02	78.5	80	0.02	-2	-5	55.9	16	19	73	99
IR18-02	80	81.2	7.00E-03	-2	-5	1.7	14	11	10	24
IR18-02	81.2	82.39	0.01	-2	-5	43.3	12	22	58	599
IR18-02	82.39	83.82	9.00E-03	-2	-5	28.2	9	27	42	482
IR18-02	83.82	84.9	0.01	-2	-5	35.3	18	13	58	102
IR18-02	84.9	85.95	7.00E-03	-2	-5	11.5	17	18	70	16
IR18-02	85.95	87.15	0.02	-2	-5	8.8	16	17	63	19
IR18-02	87.15	88.27	0.01	-2	-5	11	19	17	47	45
IR18-02	88.27	89.9	9.00E-03	-2	-5	31.8	16	22	41	157
IR18-02	89.9	91.44	8.00E-03	-2	-5	99.4	6	39	61	184
IR18-02	91.44	92.96	6.00E-03	-2	-5	34.3	6	13	77	64
IR18-02	92.96	94.55	7.00E-03	-2	-5	18.5	6	12	73	67
IR18-02	94.55	96.12	7.00E-03	-2	-5	37.3	18	18	154	90
IR18-02	96.12	97.49	0.01	-2	-5	37.1	8	63	92	279
IR18-02	97.49	99.01	9.00E-03	-2	-5	7.5	15	12	38	16
IR18-02	99.01	100.5	0.01	-2	-5	9.3	28	18	50	36
IR18-02	100.5	102.11	0.02	-2	-5	17.3	13	25	38	39
IR18-02	102.11	103.6	0.01	-2	17	74.3	6	136	40	227
IR18-02	103.6	105.16	0.07	-2	-5	17.9	9	24	49	121
IR18-02	105.16	106.35	0.01	-2	-5	4.7	16	16	36	32
IR18-02	106.35	107.5	8.00E-03	-2	-5	1.3	19	14	37	29
IR18-02	107.5	108.75	5.00E-03	-2	-5	0.9	18	16	36	51
IR18-02	108.75	109.5	1.34	-2	-5	14	15	59	46	1170
IR18-02	109.5	111	0.19	-2	-5	10.9	26	43	25	813
IR18-02	111	112.8	0.04	-2	-5	24.9	18	41	52	279
IR18-02	112.8	114	0.01	-2	-5	22.1	22	28	50	91

Hole ID	Depth from (m)	Depth to (m)	Au (ppm)	Ag (ppm)	Bi (ppm)	Cu (ppm)	Pb (ppm)	Sb (ppm)	Zn (ppm)	As (ppm)
IR18-02	114	115.15	7.00E-03	-2	-5	18.7	13	27	93	52
IR18-02	115.15	116.28	-5.00E-03	-2	-5	8.7	14	28	95	56
IR18-02	116.28	117.8	-5.00E-03	-2	-5	8.3	10	12	109	20
IR18-02	117.8	119	8.00E-03	-2	-5	24.1	18	11	89	97
IR18-02	119	120.5	0.01	-2	-5	29.4	13	6	76	24
IR18-02	122	123.44	8.00E-03	-2	-5	25.4	24	9	43	42
IR18-02	123.44	125	7.00E-03	-2	-5	7.2	33	9	19	24
IR18-02	125	126.49	0.01	-2	-5	29.7	19	7	30	15
IR18-02	126.5	128	8.00E-03	-2	-5	10.3	21	9	38	24
IR18-02	128	129.54	0.01	-2	-5	9.6	21	9	46	34
IR18-02	129.54	131.36	0.01	-2	-5	56.3	41	11	76	44
IR18-02	131.36	132.8	0.01	-2	-5	14.8	30	11	42	46
IR18-02	132.8	134.11	0.02	-2	-5	16.9	31	8	186	79
IR18-02	134.11	135.65	0.04	-2	-5	72.7	45	12	84	318
IR18-02	135.7	137.16	0.04	-2	-5	53.8	137	13	352	582
IR18-02	137.16	138.6	0.02	-2	-5	18.2	30	10	34	55
IR18-02	138.6	140.21	0.05	3	8	70.9	326	11	565	457
IR18-02	140.21	141.75	0.03	-2	-5	60.8	52	11	126	254
IR18-02	141.75	143.26	8.00E-03	-2	-5	107	15	9	15	14
IR18-02	143.26	145.75	7.00E-03	-2	-5	10.3	13	6	14	-3
IR18-02	145.75	146.3	-5.00E-03	-2	-5	11.9	12	7	14	-3
IR18-02	146.3	147.8	0.01	-2	-5	12.5	12	5	17	-3
IR18-02	147.8	149.35	7.00E-03	-2	-5	17.8	13	8	18	-3
IR18-02	149.35	150.9	-5.00E-03	-2	-5	9.1	13	6	18	-3
IR18-02	150.9	152.4	-5.00E-03	-2	-5	24.8	16	7	21	5
IR18-02	152.4	154	9.00E-03	-2	-5	30.4	16	7	26	-3
IR18-02	154	155.45	-5.00E-03	-2	-5	26.8	14	7	22	-3
IR18-02	155.45	157	8.00E-03	-2	-5	64.4	14	8	21	-3
IR18-02	157	158.5	8.00E-03	-2	-5	85.1	14	8	24	3
IR18-02	158.5	160	6.00E-03	-2	-5	10.8	15	8	31	-3
IR18-02	160	161.54	0.01	-2	-5	202	13	7	27	9
IR18-02	161.54	163.1	0.02	-2	-5	398	13	7	29	-3
IR18-02	163.1	164.59	9.00E-03	-2	-5	109	14	8	26	-3
IR18-02	164.6	166.25	6.00E-03	-2	-5	34.1	13	8	26	-3
IR18-02	166.25	167.9	6.00E-03	-2	-5	10	14	6	24	-3
IR18-02	167.9	169.5	0.01	-2	-5	485	20	42	32	38
IR18-02	169.5	171	0.05	-2	-5	12.2	34	11	18	280
IR18-02	171	172.4	0.04	-2	-5	13.6	28	12	19	505
IR18-02	172.4	173.74	0.01	-2	-5	11.6	25	10	19	197
IR18-02	173.74	175.26	0.01	-2	-5	35.3	26	9	28	102
IR18-03	52.86	54.35	9.00E-03	-2	-5	57.2	19	10	48	32
IR18-03	54.35	55.89	5.00E-03	-2	-5	22.7	11	6	22	121
IR18-03	55.89	57.3	6.00E-03	-2	-5	14.2	21	13	51	128
IR18-03	57.3	59	0.01	-2	-5	8.9	77	17	248	73
IR18-03	59	60.5	0.02	3	-5	12.4	1510	13	735	64
IR18-03	60.5	62	0.01	-2	-5	27.4	634	24	779	119
IR18-03	62	63.5	0.01	-2	-5	7.8	27	11	117	16
IR18-03	63.5	64.9	0.01	-2	-5	54.5	80	8	166	74
IR18-03	64.9	66.5	0.01	-2	-5	32.9	14	10	51	58
IR18-03	66.5	67.75	9.00E-03	-2	-5	1.7	19	11	53	17
IR18-03	67.75	69.1	0.01	-2	-5	9.8	17	8	49	16
IR18-03	69.1	70.5	0.01	-2	-5	18.2	22	18	50	149
IR18-03	70.5	71.75	0.01	-2	-5	19.7	121	24	464	61

Hole ID	Depth from (m)	Depth to (m)	Au (ppm)	Ag (ppm)	Bi (ppm)	Cu (ppm)	Pb (ppm)	Sb (ppm)	Zn (ppm)	As (ppm)
IR18-03	71.75	73	0.01	5	17	13.8	382	15	495	24
IR18-03	73	74	9.00E-03	-2	-5	50.7	35	20	92	18
IR18-03	74	75	0.02	26	41	1940	1340	465	511	422
IR18-03	75	76.1	0.02	5	26	277	269	84	249	111
IR18-03	76.1	77.18	0.55	-2	-5	12	17	43	56	2120
IR18-03	77.18	78.18	1.28	-2	-5	8.1	8	61	23	1490
IR18-03	78.18	78.8	0.99	-2	-5	9.7	11	51	27	1060
IR18-03	78.8	79.65	0.44	-2	-5	8.3	9	43	40	661
IR18-03	79.65	80.6	0.01	-2	-5	19.1	4	36	44	72
IR18-03	80.6	81.8	0.03	-2	-5	13	6	35	54	165
IR18-03	81.8	82.5	2.2	-2	-5	7.8	9	38	30	1400
IR18-03	82.5	83.95	2.12	-2	-5	7.2	13	40	26	2140
IR18-03	83.95	84.95	0.86	-2	-5	5.9	12	33	37	1080
IR18-03	84.95	85.83	0.14	-2	-5	7.1	17	39	32	251
IR18-03	85.83	86.6	0.03	-2	-5	3	24	40	28	123
IR18-03	86.6	87.36	0.09	-2	-5	6.2	18	39	28	242
IR18-03	87.36	88.39	1.21	-2	-5	11.1	11	58	35	1610
IR18-03	88.39	89.19	2.72	-2	-5	9.9	18	44	25	1770
IR18-03	89.19	90	0.03	-2	-5	-0.5	21	22	30	23
IR18-03	90	91	0.02	-2	-5	1.4	34	24	22	24
IR18-03	91	91.8	0.01	-2	-5	4.2	35	26	20	103
IR18-03	91.8	92.7	0.01	-2	-5	8.9	32	29	18	78
IR18-03	92.7	93.71	0.01	-2	-5	4	29	24	12	42
IR18-03	93.71	94.6	0.01	-2	-5	16.8	18	36	36	160
IR18-03	94.6	95.3	-5.00E-03	-2	-5	5.5	8	25	26	80
IR18-03	95.3	96	0.28	-2	-5	21.7	8	35	32	952
IR18-03	96	97	0.08	-2	-5	22.9	8	29	27	571
IR18-03	97	97.8	0.01	-2	-5	49.4	117	29	180	124
IR18-03	97.8	98.65	0.04	-2	-5	12.2	14	23	29	399
IR18-03	98.65	99.65	0.85	-2	-5	12	9	51	30	3590
IR18-03	99.65	100.5	0.01	-2	-5	25	37	35	15	218
IR18-03	100.5	101.1	-5.00E-03	-2	-5	12.7	21	25	22	106
IR18-03	101.1	101.85	0.24	-2	-5	104	83	46	132	2170
IR18-03	101.85	102.85	1.75	10	23	417	366	161	840	10000
IR18-03	102.85	103.75	0.56	7	15	254	280	93	610	9910
IR18-03	103.75	104.65	1.29	24	29	456	3940	89	7710	10000
IR18-03	104.65	105.62	7.00E-03	-2	-5	18.9	23	21	72	113
IR18-03	105.62	107	8.00E-03	-2	-5	7.7	18	14	64	227
IR18-03	107	108.5	6.00E-03	-2	-5	10	17	11	54	10
IR18-03	108.5	110	8.00E-03	-2	-5	6	16	10	55	10
IR18-03	110	111.5	-5.00E-03	-2	-5	5.1	17	8	53	4
IR18-03	111.5	113	-5.00E-03	-2	-5	8.1	13	9	62	9
IR18-03	114.5	115.6	-5.00E-03	-2	-5	5.8	14	8	80	5
IR18-03	115.6	116.76	-5.00E-03	-2	-5	9.4	14	8	75	-3
IR18-04	1.4	4.57	-5.00E-03	2	-5	25.9	10	16	67	13
IR18-04	4.57	6.1	-5.00E-03	-2	-5	16.8	12	17	79	48
IR18-04	6.1	7.62	-5.00E-03	-2	-5	14.3	9	14	57	18
IR18-04	7.62	9.14	0.02	-2	-5	39.1	66	29	58	361
IR18-04	9.14	10.67	7.00E-03	-2	-5	-0.5	13	18	70	39
IR18-04	10.67	12.19	0.01	-2	-5	2.3	106	15	88	56
IR18-04	12.19	13.72	0.02	-2	-5	17.2	17	17	80	35
IR18-04	13.72	15.24	0.01	-2	-5	3.3	26	14	76	11
IR18-04	15.24	16.76	0.13	-2	-5	1.6	152	10	193	12

Hole ID	Depth from (m)	Depth to (m)	Au (ppm)	Ag (ppm)	Bi (ppm)	Cu (ppm)	Pb (ppm)	Sb (ppm)	Zn (ppm)	As (ppm)
IR18-04	16.76	18.29	0.01	-2	-5	0.8	13	9	51	8
IR18-04	18.29	19.81	5.00E-03	-2	-5	-0.5	10	11	46	8
IR18-04	19.81	21.34	-5.00E-03	-2	-5	1.8	9	14	65	15
IR18-04	21.34	22.86	7.00E-03	-2	-5	12.9	5	25	43	38
IR18-04	22.86	24.38	8.00E-03	-2	-5	14.2	6	17	49	14
IR18-04	24.38	25.91	-5.00E-03	-2	-5	6.1	11	11	58	8
IR18-04	25.91	27.43	-5.00E-03	-2	-5	-0.5	11	11	59	-3
IR18-04	27.43	28.96	6.00E-03	-2	-5	2.3	14	11	59	-3
IR18-04	28.96	30.48	-5.00E-03	-2	-5	4.5	11	11	71	-3
IR18-04	30.48	32	8.00E-03	-2	-5	21.2	12	14	62	14
IR18-04	32	33.53	-5.00E-03	-2	-5	3	12	11	56	6
IR18-04	33.53	35.05	9.00E-03	-2	-5	6.8	11	14	56	11
IR18-04	35.05	36.58	0.02	-2	-5	5.5	10	16	48	10
IR18-04	36.58	38.1	7.00E-03	-2	-5	5.7	9	14	48	4
IR18-04	38.1	39.62	-5.00E-03	-2	-5	3.8	12	14	51	5
IR18-04	39.62	41.15	7.00E-03	-2	-5	4.3	10	14	39	4
IR18-04	41.15	42.67	0.01	-2	-5	7.3	14	15	50	13
IR18-04	42.67	44.2	0.02	-2	-5	36.8	41	13	306	61
IR18-04	44.2	45.72	0.01	-2	-5	14.1	17	10	61	21
IR18-04	45.72	47.24	0.03	-2	-5	14.9	12	14	74	13
IR18-04	47.24	47.95	0.38	-2	-5	12.6	13	14	77	14
IR18-04	47.95	49	0.1	-2	-5	104	64	26	78	109
IR18-04	49	50.29	8.00E-03	-2	-5	-0.5	12	11	83	-3
IR18-04	50.29	51.82	8.00E-03	-2	-5	-0.5	15	13	88	4
IR18-04	51.82	53.34	9.00E-03	-2	-5	-0.5	14	11	84	8
IR18-04	53.34	54.86	0.02	-2	-5	3.2	13	9	83	26
IR18-04	54.86	56.39	6.00E-03	-2	-5	9.7	16	13	79	12
IR18-04	56.39	57.91	7.00E-03	-2	-5	4.5	16	11	76	4
IR18-04	57.91	59.44	6.00E-03	-2	-5	3.4	16	11	80	9
IR18-04	59.44	60.96	6.00E-03	-2	-5	4.5	16	10	69	-3
IR18-04	60.96	62.48	0.01	-2	-5	4.4	23	11	36	10
IR18-04	62.48	63.9	0.01	-2	-5	12.7	16	12	56	11
IR18-04	63.9	65.45	0.01	-2	-5	26.6	12	11	116	42
IR18-04	65.45	67.06	-5.00E-03	-2	-5	5.1	13	12	74	28
IR18-04	67.06	68.58	5.00E-03	-2	-5	2	12	11	73	67
IR18-04	68.58	70.1	0.01	-2	-5	4.8	10	10	76	38
IR18-04	70.1	71.63	0.05	-2	-5	194	14	17	99	50
IR18-04	71.63	73.15	0.01	-2	-5	12.8	8	18	34	19
IR18-04	73.15	74.68	6.00E-03	-2	-5	7.7	12	17	50	29
IR18-04	74.68	76.2	0.01	-2	-5	15.4	12	15	43	39
IR18-04	76.2	77.72	0.01	-2	-5	29.3	10	18	41	25
IR18-04	77.72	79	0.01	-2	-5	6.7	14	14	58	18
IR18-04	80.25	81.5	0.04	-2	-5	25.9	14	17	96	54
IR18-04	81.5	82.86	0.03	-2	-5	17.4	13	17	103	55
IR18-04	82.86	84.1	0.01	-2	-5	20.9	12	11	57	15
IR18-04	84.1	85.5	0.03	-2	-5	40.4	13	11	48	26
IR18-04	85.5	86.87	0.02	-2	-5	57.5	16	15	70	22
IR18-04	86.87	88.15	0.02	-2	-5	35	14	11	65	17
IR18-04	88.15	89.15	0.01	-2	-5	4	9	13	112	8
IR18-04	89.15	90.5	0.01	-2	-5	15.6	13	10	59	8
IR18-04	90.5	92	0.01	-2	-5	5.7	16	12	61	22
IR18-04	92	93.5	0.01	-2	-5	6.2	15	13	70	28
IR18-04	93.5	95	0.01	-2	-5	5	25	14	38	19

Hole ID	Depth from (m)	Depth to (m)	Au (ppm)	Ag (ppm)	Bi (ppm)	Cu (ppm)	Pb (ppm)	Sb (ppm)	Zn (ppm)	As (ppm)
IR18-04	95	96.5	0.02	-2	-5	8.3	21	17	71	62
IR18-04	96.5	98	0.07	-2	-5	6.7	22	16	63	54
IR18-04	98	99.5	0.02	-2	-5	12.5	17	14	69	53
IR18-04	99.5	101	0.01	-2	-5	4.7	14	12	66	36
IR18-04	101	102.5	9.00E-03	-2	-5	5.2	13	9	64	11
IR18-04	102.5	104	0.02	-2	-5	4.6	12	11	64	13
IR18-04	104	105.16	0.02	-2	-5	4.4	12	8	60	14
IR18-04	105.16	106.5	0.08	-2	-5	22.1	20	14	70	71
IR18-04	106.5	108	0.21	-2	-5	51.9	20	16	74	66
IR18-04	108	109.5	0.1	-2	-5	4.9	13	10	58	21
IR18-04	109.5	111	0.29	-2	-5	18.7	12	14	58	34
IR18-04	111	112.5	0.03	-2	-5	11.9	11	12	57	26
IR18-04	112.5	113.6	0.03	-2	-5	13.6	12	14	66	22
IR18-04	113.6	114.74	2.36	-2	-5	18.8	12	11	53	18
IR18-04	114.74	116.24	0.22	-2	-5	9.8	10	10	31	174
IR18-04	116.24	117.5	0.01	-2	-5	26.4	9	18	28	256
IR18-04	117.5	118.6	0.01	-2	-5	18.7	5	12	25	138
IR18-04	118.6	119.81	0.01	-2	-5	37.7	11	18	30	134
IR18-04	119.81	121.25	0.01	-2	-5	8.4	16	14	65	178
IR18-04	121.25	122.55	0.01	-2	-5	11	16	11	74	32
IR18-04	122.55	124	0.02	-2	-5	22.2	15	10	69	25
IR18-04	124	125.5	0.05	-2	-5	111	16	22	66	242
IR18-04	125.5	127	0.02	-2	-5	31.2	15	16	64	66
IR18-04	127	128.5	0.01	-2	-5	10.7	14	16	64	21
IR18-04	128.5	130	0.02	-2	-5	6.6	13	15	65	21
IR18-04	130	131.5	0.03	-2	-5	6.3	12	17	58	23
IR18-04	131.5	133	0.01	-2	-5	0.8	14	17	64	25
IR18-04	133	134.5	0.02	-2	-5	2.8	14	25	69	35
IR18-04	134.5	136	0.01	-2	-5	2.2	13	20	61	22
IR18-04	136	137.5	0.03	-2	-5	5.7	15	18	73	30
IR18-04	137.5	139	0.06	-2	-5	4.3	16	20	72	153
IR18-04	139	140.5	0.02	-2	-5	1.2	15	20	69	29
IR18-04	140.5	142.03	0.01	-2	-5	2.9	17	22	69	24
IR18-04	142.03	143.13	0.03	-2	-5	2.5	27	20	29	22
IR18-04	143.13	144.12	0.01	-2	-5	3.3	18	22	58	23
IR18-04	144.12	145.15	0.01	-2	-5	11.5	11	24	68	20
IR18-04	145.15	146.1	0.01	-2	-5	8.9	13	20	53	23
IR18-04	146.1	146.95	0.02	-2	-5	10.7	13	23	59	20
IR18-04	146.95	147.83	0.02	-2	-5	21.3	16	23	71	30
IR18-04	147.83	149.35	8.00E-03	-2	-5	12.3	13	15	63	16
IR18-04	149.35	150.35	0.01	-2	-5	20.1	11	12	54	20
IR18-04	150.35	151.26	0.02	-2	-5	17.9	12	12	54	33
IR18-04	151.26	152.5	-5.00E-03	-2	-5	14	14	12	29	9
IR18-04	152.5	154	8.00E-03	-2	-5	21	11	12	21	-3
IR18-04	154	155.5	8.00E-03	-2	-5	6.2	12	10	22	4
IR18-04	155.5	157	5.00E-03	-2	-5	4.9	14	9	24	5
IR18-04	157	158.5	5.00E-03	-2	-5	2.1	10	8	26	35
IR18-04	158.5	160	5.00E-03	-2	-5	5	11	8	29	3
IR18-04	160	161	-5.00E-03	-2	-5	3	11	9	33	-3
IR18-04	161	162	6.00E-03	-2	-5	10.5	15	10	226	-3
IR18-04	162	162.9	0.02	-2	-5	33.5	228	13	798	26
IR18-04	162.9	163.8	0.08	-2	-5	55.9	200	10	1800	111
IR18-04	163.8	164.8	0.01	-2	-5	24.2	76	12	236	123

Hole ID	Depth from (m)	Depth to (m)	Au (ppm)	Ag (ppm)	Bi (ppm)	Cu (ppm)	Pb (ppm)	Sb (ppm)	Zn (ppm)	As (ppm)
IR18-04	164.8	166.12	6.00E-03	-2	-5	3.2	10	8	91	12
IR18-04	166.12	167.5	9.00E-03	-2	-5	15.6	12	10	50	-3
IR18-04	167.5	169	-5.00E-03	-2	-5	16.9	14	8	29	-3
IR18-04	169	170.5	8.00E-03	-2	-5	2.1	14	7	22	-3
IR18-04	170.5	172	5.00E-03	-2	-5	20.9	17	8	19	9
IR18-04	172	173.5	0.05	-2	-5	87.4	14	13	63	110
IR18-04	173.5	175	6.00E-03	-2	-5	13.6	17	9	47	18
IR18-04	196	197.5	8.00E-03	-2	-5	33	15	13	70	26
IR18-04	197.5	199	0.01	-2	19	166	121	12	221	24
IR18-04	199	200.5	0.03	-2	-5	95.9	23	10	77	47
IR18-05	22	23.5	-5.00E-03	-2	-5	9.4	14	12	36	44
IR18-05	23.5	25	-5.00E-03	-2	-5	4.7	12	16	57	5
IR18-05	25	26.5	-5.00E-03	-2	-5	5.5	13	14	66	4
IR18-05	26.5	28	0.01	-2	-5	8.2	16	17	64	6
IR18-05	28	29.5	-5.00E-03	-2	-5	4.8	13	15	48	8
IR18-05	29.5	31	5.00E-03	-2	-5	4.2	12	18	54	32
IR18-05	31	40.6	-5.00E-03	-2	-5	-0.5	17	6	41	-3
IR18-05	40.6	42	-5.00E-03	-2	-5	34.1	10	22	34	83
IR18-05	42	43	-5.00E-03	-2	-5	42.3	6	28	25	66
IR18-05	43	43.9	0.01	-2	-5	68.6	9	45	31	165
IR18-05	43.9	44.9	1.3	-2	-5	11.3	15	71	54	4770
IR18-05	44.9	45.6	0.32	-2	-5	20.7	10	53	42	3200
IR18-05	45.6	46.2	0.35	-2	-5	7.2	12	52	55	624
IR18-05	46.2	47.2	4.53	-2	-5	7.8	9	60	68	4200
IR18-05	47.2	48.2	0.42	-2	-5	13.4	12	47	48	802
IR18-05	48.2	49	0.05	-2	-5	2.3	9	28	41	186
IR18-05	49	49.98	0.02	-2	-5	7	11	32	49	208
IR18-05	49.98	50.9	0.29	-2	-5	6.9	13	42	66	1120
IR18-05	50.9	51.9	0.74	-2	-5	7.2	13	52	55	1560
IR18-05	51.9	52.9	0.59	-2	-5	16.7	13	65	56	3790
IR18-05	52.9	53.9	0.91	-2	-5	10.7	9	56	46	2750
IR18-05	53.9	54.9	0.07	-2	-5	4	11	32	59	512
IR18-05	54.9	55.9	2.62	-2	-5	5.8	13	61	60	3260
IR18-05	55.9	56.9	2.73	-2	-5	8	17	91	54	4290
IR18-05	56.9	57.9	0.57	-2	-5	13.2	6	50	19	961
IR18-05	57.9	58.9	0.55	-2	-5	44.1	12	82	19	2130
IR18-05	58.9	59.9	0.15	-2	-5	32.3	18	47	26	577
IR18-05	59.9	60.9	0.47	-2	-5	8.9	14	48	33	954
IR18-05	60.9	61.9	4.3	-2	-5	7.2	7	47	39	3230
IR18-05	61.9	62.9	1.02	-2	-5	7.9	11	32	28	1410
IR18-05	62.9	63.9	0.01	-2	-5	10.9	20	25	21	65
IR18-05	63.9	65	0.04	-2	-5	4	14	13	23	26
IR18-05	65	66.5	7.00E-03	-2	-5	2.2	13	20	25	28
IR18-05	66.5	67.5	6.00E-03	-2	-5	10.6	22	22	23	33
IR18-05	67.5	68.58	0.01	-2	-5	31	8	27	31	55
IR18-05	68.58	70	6.00E-03	-2	-5	20.8	9	11	42	71
IR18-05	70	71.5	9.00E-03	-2	-5	19	10	24	66	74
IR18-05	71.5	73	0.01	-2	-5	52.4	18	37	86	70
IR18-05	73	74.5	0.01	-2	-5	37.2	8	38	29	77
IR18-05	74.5	76	0.04	-2	-5	36.6	11	33	39	106
IR18-05	76	77.5	0.02	-2	-5	19.4	10	29	40	101
IR18-05	77.5	79	9.00E-03	-2	-5	29.7	22	36	28	58
IR18-05	79	80.4	0.01	-2	-5	29.6	25	33	38	69

Hole ID	Depth from (m)	Depth to (m)	Au (ppm)	Ag (ppm)	Bi (ppm)	Cu (ppm)	Pb (ppm)	Sb (ppm)	Zn (ppm)	As (ppm)
IR18-05	80.4	81.41	0.02	-2	-5	9.8	24	28	40	41
IR18-05	81.41	82.9	0.01	-2	-5	4.9	46	25	61	30
IR18-05	82.9	84.4	-5.00E-03	-2	-5	4.1	20	16	50	36
IR18-05	84.4	85.9	7.00E-03	-2	-5	13.4	14	26	68	54
IR18-05	85.9	86.87	0.49	-2	-5	16.7	12	44	43	2430
IR18-05	86.87	88.39	0.01	-2	-5	3.8	16	27	55	49
IR18-05	88.39	89.92	0.01	-2	-5	4.8	19	28	55	36
IR18-05	94.49	96.01	0.02	-2	-5	12	17	19	45	90
IR18-05	96.01	97.54	0.01	-2	-5	13.9	15	17	49	38
IR18-05	97.54	99.06	0.01	-2	-5	20.4	16	18	43	37
IR18-06	9.14	10.67	9.00E-03	-2	-5	37.1	11	18	33	263
IR18-06	10.67	12.19	8.00E-03	-2	-5	20	12	13	35	99
IR18-06	16.76	18.29	0.01	-2	-5	47.3	11	14	26	147
IR18-06	18.29	19.81	0.03	-2	-5	44.4	14	17	22	2910
IR18-06	26.65	28.15	0.01	-2	-5	19.5	24	33	45	83
IR18-06	28.15	29.65	0.01	-2	-5	9.4	12	27	72	76
IR18-06	33.53	35.05	-5.00E-03	-2	-5	21.3	21	26	63	296
IR18-06	35.05	36.58	5.00E-03	-2	-5	3.4	29	26	83	215
IR18-06	36.58	38.1	8.00E-03	-2	-5	-0.5	31	13	86	139
IR18-06	38.1	39.2	0.02	-2	-5	6.6	17	20	54	159
IR18-06	39.2	40.35	0.01	-2	-5	3	24	18	40	68
IR18-06	40.35	41.46	0.01	-2	-5	5.7	32	26	30	128
IR18-06	41.46	42.67	9.00E-03	-2	-5	15.4	35	50	56	45
IR18-06	42.67	44.2	0.02	-2	-5	11.1	43	55	44	177
IR18-06	44.2	45.72	0.07	-2	-5	9.7	38	38	34	239
IR18-06	45.72	46.7	9.00E-03	-2	-5	11.8	33	24	36	75
IR18-06	46.7	47.62	-5.00E-03	-2	-5	13.1	22	35	38	30
IR18-06	47.62	49	0.08	-2	-5	25.5	34	37	59	122
IR18-06	49	50.64	0.05	-2	-5	28.5	27	22	62	170
IR18-06	50.64	52.13	0.01	-2	-5	19.5	41	22	50	37
IR18-06	52.13	53.34	7.00E-03	-2	-5	13.9	24	15	42	31
IR18-06	53.34	54.86	0.01	-2	-5	27.3	23	14	54	56
IR18-06	54.86	56.39	9.00E-03	-2	-5	8.5	25	26	52	111
IR18-06	56.39	57.25	0.01	-2	-5	7.1	7	27	55	82
IR18-06	57.25	58.25	1.34	-2	-5	8.2	14	64	112	4190
IR18-06	58.25	59.6	0.03	-2	-5	6.4	10	26	42	65
IR18-06	59.6	61.2	0.02	-2	-5	16.1	11	28	45	36
IR18-06	61.2	62.48	9.00E-03	-2	-5	9.8	18	28	38	41
IR18-06	62.48	63.54	0.01	-2	-5	6.3	47	32	69	26
IR18-06	63.54	65.2	0.01	-2	-5	14	7	30	50	48
IR18-06	65.2	66.48	0.05	-2	-5	25.1	8	33	94	363
IR18-06	66.48	67.75	0.01	-2	-5	24.9	10	51	125	212
IR18-06	67.75	68.75	0.53	-2	-5	8.1	14	79	47	831
IR18-06	68.75	69.7	0.8	-2	-5	11.5	20	80	52	1910
IR18-06	69.7	70.7	0.69	-2	-5	7.1	15	79	32	1050
IR18-06	70.7	71.72	0.69	-2	-5	16.6	15	96	35	1120
IR18-06	71.72	72.68	1.73	-2	-5	16.1	21	103	60	7770
IR18-06	72.68	73.58	0.7	-2	-5	11.7	31	70	35	3360
IR18-06	73.58	74.45	1.21	-2	-5	14.2	16	78	69	4030
IR18-06	74.45	75.45	0.26	-2	-5	26.4	34	71	61	1220
IR18-06	75.45	77	0.03	-2	-5	1.7	29	63	54	118
IR18-06	77	78.5	7.00E-03	-2	-5	4.7	22	66	29	29
IR18-06	78.5	80	0.01	-2	-5	24.1	34	107	22	13

Appendix 2b. (*Contd.*)

Hole ID	Depth from (m)	Depth to (m)	Au (ppm)	Ag (ppm)	Bi (ppm)	Cu (ppm)	Pb (ppm)	Sb (ppm)	Zn (ppm)	As (ppm)
IR18-06	80	81.5	8.00E-03	-2	-5	42.3	64	61	25	25
IR18-06	81.5	83	0.01	-2	-5	17.5	29	25	70	17
IR18-06	83	84.5	0.04	-2	-5	19.5	24	29	39	42
IR18-06	84.5	86	7.00E-03	-2	-5	2	27	9	29	12
IR18-06	86	87.2	-5.00E-03	-2	-5	8.2	21	11	33	-3
IR18-06	87.2	88.62	6.00E-03	-2	-5	13.2	15	11	66	6
IR18-06	88.62	89.99	8.00E-03	-2	-5	111	17	12	70	21
IR18-06	89.99	91.44	0.02	-2	-5	47.5	21	14	61	9
IR18-06	91.44	92.96	-5.00E-03	-2	-5	15.9	13	13	72	-3
IR18-06	92.96	94.49	6.00E-03	-2	-5	9.5	19	11	48	-3
IR18-06	94.49	95.75	5.00E-03	-2	-5	14.4	19	14	63	-3
IR18-06	95.75	97.25	7.00E-03	-2	-5	86.4	19	10	83	6
IR18-06	97.25	98.75	6.00E-03	-2	-5	25	12	9	70	8
IR18-06	98.75	100.21	8.00E-03	-2	-5	18.3	14	11	72	16
IR18-07	15.24	16.76	0.01	-2	-5	36.3	21	19	30	31
IR18-07	16.76	18.29	0.01	-2	-5	11.7	23	24	29	52
IR18-07	18.29	19.47	0.01	-2	-5	18	12	25	32	106
IR18-07	38.3	39.72	8.00E-03	-2	-5	34	16	11	52	93
IR18-07	39.72	40.7	8.00E-03	-2	-5	11.5	23	22	22	85
IR18-07	40.7	41.45	0.04	-2	-5	41.3	17	39	31	418
IR18-07	41.45	42.2	7.00E-03	-2	-5	35.2	8	15	22	97
IR18-07	42.2	43.8	0.01	-2	-5	32	8	12	36	81
IR18-07	43.8	45.48	5.00E-03	-2	-5	9.8	15	10	45	31
IR18-07	45.48	47	7.00E-03	-2	-5	18	15	13	55	80
IR18-07	47	48.5	7.00E-03	-2	-5	20.7	20	18	39	322
IR18-07	48.5	49.7	6.00E-03	-2	-5	30.1	13	13	49	175
IR18-07	49.7	50.93	7.00E-03	-2	-5	13.9	15	16	23	82
IR18-07	50.93	52.45	5.00E-03	-2	-5	21.6	6	10	102	46
IR18-07	52.45	54	0.01	-2	-5	34.2	12	26	29	88
IR18-07	54	55.5	8.00E-03	-2	-5	39.3	16	15	29	121
IR18-07	55.5	57	0.01	-2	-5	24.9	16	14	32	120
IR18-07	57	58.65	0.01	-2	-5	11.9	29	32	103	89
IR18-07	58.65	59.65	0.01	-2	-5	30.3	27	25	137	139
IR18-07	59.65	60.96	0.01	-2	-5	48.6	42	44	143	124
IR18-07	60.96	62.48	0.01	-2	-5	40.5	25	34	313	263
IR18-07	62.48	64.01	0.01	-2	-5	43.6	47	25	278	275
IR18-07	64.01	65.53	0.06	-2	-5	90.5	83	37	325	1740
IR18-07	65.53	67.06	0.01	-2	-5	71.5	45	41	303	336
IR18-07	67.06	68.58	9.00E-03	-2	-5	17.1	17	13	73	81
IR18-07	68.58	70.1	8.00E-03	-2	-5	32.2	14	30	53	113
IR18-07	70.1	71.63	6.00E-03	-2	-5	7.8	14	16	73	76
IR18-07	71.63	73.15	7.00E-03	-2	-5	9.2	11	27	71	67
IR18-07	73.15	74.68	7.00E-03	-2	-5	5.5	19	16	37	125
IR18-07	74.68	76.2	7.00E-03	-2	-5	7.6	13	16	134	66
IR18-07	76.2	77.72	0.02	-2	-5	119	96	43	699	426
IR18-07	77.72	79.25	0.01	-2	-5	232	40	34	423	206
IR18-07	79.25	80.77	0.02	-2	-5	16.8	14	23	330	319
IR18-07	80.77	81.75	0.03	4	7	78	150	95	712	1460
IR18-07	81.75	82.72	0.09	-2	-5	59.6	267	25	686	380
IR18-07	82.72	83.71	0.81	36	137	1670	367	648	551	10000
IR18-07	83.71	84.64	0.34	7	25	757	94	217	533	9030
IR18-07	84.64	85.66	0.02	-2	-5	33.3	45	37	249	310
IR18-07	85.66	86.69	0.03	-2	-5	15	33	31	623	250

Hole ID	Depth from (m)	Depth to (m)	Au (ppm)	Ag (ppm)	Bi (ppm)	Cu (ppm)	Pb (ppm)	Sb (ppm)	Zn (ppm)	As (ppm)
IR18-07	86.69	87.68	0.02	-2	-5	15.2	29	34	370	224
IR18-07	87.68	88.68	0.01	-2	-5	5.4	11	25	317	259
IR18-07	88.68	89.75	0.09	-2	-5	14.4	14	29	140	392
IR18-07	89.75	90.75	0.01	-2	-5	15.1	11	32	123	334
IR18-07	90.75	91.75	0.1	-2	-5	30.5	88	58	295	843
IR18-07	91.75	92.75	1.85	-2	-5	13.8	72	62	186	1800
IR18-07	92.75	93.75	0.86	-2	-5	7	11	33	50	1080
IR18-07	93.75	94.75	0.39	-2	-5	21.8	28	53	61	1480
IR18-07	94.75	95.75	1.53	-2	-5	9.6	21	66	104	2420
IR18-07	95.75	96.7	0.69	-2	-5	6.5	26	65	15	199
IR18-07	96.7	97.75	0.11	-2	-5	24.1	29	91	70	177
IR18-07	97.75	98.71	0.01	-2	-5	29.1	12	50	79	62
IR18-07	98.71	100	7.00E-03	-2	-5	19.9	9	38	68	16
IR18-07	100	101.4	9.00E-03	-2	-5	27.3	13	21	60	7
IR18-07	101.4	103	0.01	-2	-5	18.7	13	12	70	-3
IR18-07	103	104.53	7.00E-03	-2	-5	37	12	13	67	10
IR18-07	104.53	106.14	6.00E-03	-2	-5	26.7	12	14	71	4
IR18-07	106.14	107.74	0.01	-2	-5	63.3	14	33	61	13
IR18-07	107.74	109	8.00E-03	-2	-5	54.9	16	20	56	13
IR18-07	109	110.46	0.01	-2	-5	98.8	14	34	68	10
IR18-07	110.46	111.93	7.00E-03	-2	-5	27.8	12	19	66	17
IR18-07	111.93	113.2	-5.00E-03	-2	-5	15.5	16	19	62	111
IR18-07	113.2	114.17	0.03	-2	-5	10.1	16	34	88	62
IR18-07	114.17	115.17	0.13	-2	-5	16.5	19	55	63	226
IR18-07	115.17	116.14	0.02	-2	-5	11.1	21	39	70	82
IR18-07	116.14	117.35	0.01	-2	-5	57.8	24	73	107	34
IR18-07	117.35	118.87	0.01	-2	-5	29.7	16	44	64	34
IR18-07	118.87	120.4	0.03	-2	-5	30.4	15	24	67	18
IR18-07	120.4	121.92	9.00E-03	-2	-5	28.3	15	26	73	14
IR18-07	121.92	123.44	0.01	-2	-5	2.4	15	27	64	16
IR18-07	123.44	124.97	0.01	-2	-5	22.2	17	33	44	26
IR18-07	124.97	126.49	8.00E-03	-2	-5	3.2	16	16	63	8
IR18-08	30.48	31.9	7.00E-03	-2	-5	22.3	28	19	117	261
IR18-08	31.9	32.72	0.11	-2	-5	30.1	25	49	85	565
IR18-08	32.72	33.7	0.98	-2	-5	10.4	7	52	56	778
IR18-08	33.7	34.6	1.68	-2	-5	11.4	6	69	43	1080
IR18-08	34.6	35.6	1.25	-2	-5	28.3	13	73	135	1370
IR18-08	35.6	36.58	3.05	-2	-5	24	12	68	86	1960
IR18-08	36.58	37.5	6.14	-2	-5	23.5	12	79	78	2910
IR18-08	37.5	38.25	2.14	-2	-5	12.1	13	72	72	1330
IR18-08	38.25	38.85	1.03	-2	-5	9	12	61	74	781
IR18-08	38.85	40	0.02	-2	-5	16.5	20	11	94	136
IR18-08	40	42.35	0.01	-2	-5	18.6	19	8	96	117
IR18-08	42.35	44.2	6.00E-03	-2	-5	9.3	20	16	67	132
IR18-08	53	54.86	0.01	-2	-5	2	22	13	28	29
IR18-08	67.6	69.58	8.00E-03	-2	-5	5.1	23	10	30	33
IR18-08	69.58	71.5	9.00E-03	-2	-5	7.2	20	14	32	32
IR18-08	71.5	73.5	8.00E-03	-2	-5	9.4	19	14	26	49
IR18-08	73.5	74.5	5.00E-03	-2	-5	5.2	18	13	32	18
IR18-08	74.5	76	0.01	-2	-5	14.3	19	16	29	55
IR18-08	76	77.5	7.00E-03	-2	-5	10.5	24	21	59	32
IR18-08	77.5	79	0.01	-2	-5	15.7	15	24	73	58
IR18-08	79	80.54	0.09	-2	-5	13.3	16	27	52	452

Appendix 2b. (*Contd.*)

Hole ID	Depth from (m)	Depth to (m)	Au (ppm)	Ag (ppm)	Bi (ppm)	Cu (ppm)	Pb (ppm)	Sb (ppm)	Zn (ppm)	As (ppm)
IR18-08	80.54	82	0.01	-2	-5	13.4	19	24	57	59
IR18-08	82	83.57	0.01	-2	-5	10.4	13	18	55	36
IR18-08	83.57	85	0.02	-2	-5	20	15	17	66	39
IR18-08	85	86.5	0.01	-2	-5	10.4	13	14	67	34
IR18-08	86.5	87.82	0.02	-2	-5	216	32	26	56	201
IR18-08	87.82	89.8	0.04	-2	-5	91.4	20	13	109	55
IR18-08	89.8	91	0.01	-2	-5	45.6	19	17	78	59
IR18-08	91	92.25	0.01	-2	-5	60.9	13	13	55	41
IR18-08	92.25	94	-5.00E-03	-2	-5	22.2	3	14	132	58
IR18-08	94	96	8.00E-03	-2	-5	49.7	2	20	82	95
IR18-08	96	98	0.02	-2	-5	59	5	14	121	70
IR18-08	98	99.5	7.00E-03	-2	-5	13.8	10	10	92	14
IR18-08	99.5	101	0.02	-2	-5	44	20	8	74	17
IR18-08	101	103	0.03	-2	-5	75.9	61	21	54	796
IR18-08	103	105	0.01	-2	-5	10.7	21	14	37	96
IR18-08	105	106.68	7.00E-03	-2	-5	8.5	18	14	26	9
IR18-09	15.24	16.76	7.00E-03	-2	-5	27	24	15	24	147
IR18-09	16.76	18.29	7.00E-03	-2	-5	50.4	21	13	35	178
IR18-09	18.29	19.81	6.00E-03	-2	-5	40.9	13	17	41	182
IR18-09	23.21	24.38	8.00E-03	-2	-5	84.9	9	15	105	55
IR18-09	24.38	25.38	0.02	-2	-5	49.7	12	17	50	385
IR18-09	30.48	32	-5.00E-03	-2	-5	135	10	18	40	250
IR18-09	32	33.53	9.00E-03	-2	-5	28.5	5	15	27	323
IR18-09	33.53	35.05	6.00E-03	-2	8	143	8	24	24	318
IR18-09	35.05	36.58	0.01	-2	103	1020	12	37	36	342
IR18-09	36.58	38.1	0.02	-2	7	134	11	30	27	305
IR18-09	38.1	39.62	7.00E-03	-2	-5	28.5	9	16	18	178
IR18-09	39.62	41.15	7.00E-03	-2	-5	31.8	17	13	30	199
IR18-09	41.15	42.67	0.02	-2	-5	41.3	16	16	36	218
IR18-09	42.67	44.2	-5.00E-03	-2	-5	8.3	15	12	42	98
IR18-09	44.2	45.72	6.00E-03	-2	-5	14.3	11	12	45	118
IR18-09	45.72	47.24	0.01	-2	-5	120	17	15	28	106
IR18-09	47.24	48.77	6.00E-03	-2	-5	31.4	18	12	14	56
IR18-09	48.77	50.29	9.00E-03	-2	-5	19.4	18	12	22	58
IR18-09	50.29	51.82	6.00E-03	-2	-5	1.6	19	10	23	24
IR18-09	51.82	53.34	5.00E-03	-2	-5	4	17	10	26	15
IR18-09	53.34	54.86	-5.00E-03	-2	-5	18.2	17	13	23	22
IR18-09	54.86	56.08	0.02	-2	-5	43	18	11	56	37
IR18-09	56.08	57.1	0.01	-2	-5	20.8	21	11	51	63
IR18-09	57.1	58.1	0.01	-2	-5	29.4	19	11	47	94
IR18-09	58.1	59.1	0.05	-2	-5	6.3	20	25	38	133
IR18-09	59.1	60	0.01	-2	-5	5.8	6	20	53	33
IR18-09	60	60.75	0.74	-2	-5	7.1	17	54	66	2140
IR18-09	60.75	62	0.33	-2	-5	-0.5	12	43	62	1840
IR18-09	62	63.52	0.01	-2	-5	36	16	12	59	178
IR18-09	63.52	64.3	0.01	-2	-5	48.4	36	12	69	109
IR18-09	64.3	65.53	0.01	-2	-5	42.8	23	13	56	83
IR18-09	65.53	66.85	9.00E-03	-2	-5	30.4	21	19	21	63
IR18-10	22.7	24.2	5.00E-03	-2	-5	5.7	16	16	45	24
IR18-10	24.2	25.7	6.00E-03	-2	-5	52.2	14	16	36	10
IR18-10	27.43	28.96	6.00E-03	-2	-5	0.9	15	13	47	10
IR18-10	28.96	30.48	7.00E-03	-2	-5	13.5	17	11	42	27
IR18-10	40.5	42	7.00E-03	-2	-5	4.6	16	19	76	44

Hole ID	Depth from (m)	Depth to (m)	Au (ppm)	Ag (ppm)	Bi (ppm)	Cu (ppm)	Pb (ppm)	Sb (ppm)	Zn (ppm)	As (ppm)
IR18-10	42	43	5.00E-03	-2	-5	237	17	28	234	722
IR18-10	43	44	4.39	-2	-5	68.8	38	118	89	10000
IR18-10	44	45	1.79	-2	-5	10.9	26	64	60	4970
IR18-10	45	46	0.03	-2	-5	13.7	16	47	384	750
IR18-10	46	47	0.27	-2	-5	72.8	25	74	408	1180
IR18-10	47	48	0.83	-2	-5	73.4	33	81	270	2070
IR18-10	48	49	3.13	-2	-5	58.4	22	83	155	3420
IR18-10	49	50	2.38	-2	-5	39.3	23	87	111	5860
IR18-10	50	51	4.44	-2	7	216	27	111	245	9640
IR18-10	51	52	1.21	-2	-5	154	25	86	229	2360
IR18-10	52	52.65	0.59	-2	-5	91.6	25	89	206	2260
IR18-10	52.65	53.34	0.35	-2	-5	65.2	27	70	241	1360
IR18-10	53.34	54.86	0.13	-2	-5	34.6	10	40	195	1550
IR18-10	54.86	56.39	-5.00E-03	-2	-5	7.6	13	27	88	678
IR18-10	56.39	57.91	0.21	-2	-5	5	12	28	53	427
IR18-10	57.91	59.44	0.03	-2	-5	8	12	21	61	126
IR18-10	59.44	60.96	0.01	-2	-5	3.1	10	24	70	171
IR18-10	60.96	62.05	-5.00E-03	-2	-5	0.8	9	27	70	95
IR18-10	62.05	63	0.93	-2	-5	7.4	13	46	26	2910
IR18-10	63	64	0.11	-2	-5	4.9	19	32	44	798
IR18-10	64	65	0.01	-2	-5	17.4	38	27	166	69
IR18-10	65	66	7.00E-03	-2	-5	8.8	16	27	74	44
IR18-10	66	67.06	8.00E-03	-2	-5	7	10	23	47	49
IR18-10	67.06	68	0.54	-2	-5	7.3	10	43	24	884
IR18-10	68	69	0.37	-2	-5	6.1	20	31	15	470
IR18-10	69	70	2.58	-2	-5	9.9	7	50	21	2300
IR18-10	70	70.9	2.7	-2	-5	13.4	6	60	23	2930
IR18-10	70.9	71.82	3.45	-2	-5	5.9	10	73	27	4480
IR18-10	71.82	73.15	0.01	-2	-5	4.9	17	30	44	166
IR18-10	73.15	74.34	0.16	-2	-5	22.1	34	42	33	208
IR18-10	74.34	75.6	0.15	-2	-5	28.4	25	42	50	208
IR18-10	75.6	76.35	0.02	-2	-5	10.7	2	24	10	61
IR18-10	76.35	77	0.22	-2	-5	19.7	16	48	43	675
IR18-10	77	77.72	0.15	-2	-5	83.4	19	68	32	292
IR18-10	77.72	79.25	0.01	-2	-5	6.5	31	26	29	81
IR18-10	79.25	80.77	0.02	-2	-5	14.4	36	23	34	32
IR18-10	80.77	81.4	0.01	-2	-5	8.5	15	22	29	30
IR18-10	81.4	82	0.01	-2	-5	4.9	10	31	19	17
IR18-10	82	83	0.02	-2	-5	3.9	24	26	31	42
IR18-10	83	84	0.02	-2	-5	3.2	9	20	30	41
IR18-10	84	85	0.01	-2	-5	3.9	9	22	16	14
IR18-10	85	86	0.01	-2	-5	12.8	11	25	32	35
IR18-10	86	86.87	0.01	-2	-5	10	31	18	51	41
IR18-10	86.87	88.39	6.00E-03	-2	-5	9.3	15	17	27	31
IR18-10	88.39	89.92	8.00E-03	-2	-5	13.9	21	24	35	63
IR18-10	89.92	91.44	0.01	-2	-5	12.6	24	31	22	34
IR18-10	91.44	92.96	0.01	-2	-5	43.3	11	25	53	184
IR18-10	92.96	94.49	0.02	-2	-5	61.2	19	23	40	67
IR18-10	94.49	95.4	0.01	-2	-5	27.6	12	25	25	30
IR18-10	95.4	96.3	0.02	-2	-5	15.5	7	21	48	21
IR18-10	96.3	97.54	0.02	-2	-5	29.3	21	23	49	57
IR18-10	114.3	115.82	0.02	-2	-5	61.6	10	17	67	98
IR18-10	115.82	117.35	0.02	-2	8	105	13	13	72	124

Hole ID	Depth from (m)	Depth to (m)	Au (ppm)	Ag (ppm)	Bi (ppm)	Cu (ppm)	Pb (ppm)	Sb (ppm)	Zn (ppm)	As (ppm)
IR18-10	117.35	118.87	0.03	-2	-5	25.9	14	10	36	75
IR18-11	17.25	18.75	0.01	-2	-5	5.5	13	14	48	10
IR18-11	18.75	20.25	0.02	-2	-5	5.8	9	20	51	33
IR18-11	20.25	21.75	5.00E-03	-2	-5	9.9	11	14	54	10
IR18-11	28.3	29.4	0.01	-2	-5	133	14	46	93	139
IR18-11	29.4	30.48	0.04	-2	-5	76.6	8	27	29	78
IR18-11	30.48	32	6.00E-03	-2	-5	93.2	7	16	36	19
IR18-11	32	33.53	6.00E-03	-2	-5	80.7	22	18	40	24
IR18-11	33.53	35.05	9.00E-03	-2	-5	40.8	12	22	19	264
IR18-11	35.05	36.58	0.01	-2	-5	90	12	34	17	425
IR18-11	36.58	38.1	7.00E-03	-2	-5	45.3	29	20	45	175
IR18-11	38.1	39.62	5.00E-03	-2	-5	41.7	4	18	23	97
IR18-11	39.62	41.15	7.00E-03	-2	-5	26.3	8	24	25	58
IR18-11	41.15	42.67	9.00E-03	-2	-5	93.8	9	25	33	434
IR18-11	42.67	44.2	9.00E-03	-2	-5	20.5	22	13	13	100
IR18-11	44.2	45.3	5.00E-03	-2	-5	24.5	20	10	39	76
IR18-11	45.3	46.4	6.00E-03	-2	-5	54.5	22	10	33	140
IR18-11	46.4	47.5	0.01	-2	-5	108	8	7	29	171
IR18-11	47.5	48.77	5.00E-03	-2	-5	31.6	19	13	72	32
IR18-11	62.48	64.01	0.01	-2	-5	5.4	18	18	62	40
IR18-11	64.01	65.35	0.01	-2	-5	4.8	21	15	35	37
IR18-11	65.35	66.5	0.06	-2	-5	14.5	17	20	54	150
IR18-11	66.5	67.7	0.02	-2	-5	5	15	14	38	67
IR18-11	67.7	68.88	0.01	-2	-5	7.8	10	19	35	101
IR18-11	68.88	69.82	0.03	-2	-5	69.5	71	49	77	416
IR18-11	69.82	70.75	0.01	-2	-5	19.3	15	18	64	56
IR18-11	70.75	71.63	0.01	-2	-5	12.4	15	20	202	248
IR18-11	71.63	72.66	0.01	-2	-5	64.7	22	21	3840	1370
IR18-11	72.66	73.4	6.74	9	54	1080	65	139	448	10000
IR18-11	73.4	74.41	0.03	-2	-5	73.5	27	20	230	1380
IR18-11	74.41	75.34	0.02	-2	-5	5.6	14	19	67	145
IR18-11	75.34	76.35	0.02	-2	-5	16.7	26	15	61	306
IR18-11	76.35	77.29	0.01	-2	-5	10.3	13	17	41	214
IR18-11	77.29	78.3	0.01	-2	-5	9.7	15	14	57	144
IR18-11	78.3	79.25	0.02	-2	-5	13.4	16	15	66	171
IR18-11	79.25	80.3	0.05	-2	-5	18.9	23	21	73	1110
IR18-11	80.3	81.3	0.01	-2	-5	3.9	14	13	61	71
IR18-11	81.3	82.05	0.01	-2	-5	14.6	10	19	65	128
IR18-11	82.05	83	7.00E-03	-2	-5	5.7	11	12	57	54